Adenylate cyclase activity of TIR1/AFB auxin receptors in plants

Qi, L., Kwiatkowski, M., Chen, H., Hoermayer, L., Sinclair, S., Zou, M., del Genio, C., Kubeš, M., Napier, R., Jaworski, K. & Friml, J

DOI 10.1038/s41586-022-05369-7
ISSN 0028-0836
ESSN 1476-4687

Publisher: Springer

The final publication is available at Springer via http://dx.doi.org/10.1038/s41586-022-05369-7

Adenylate cyclase activity of TIR1/AFB auxin receptors for root growth

Authors: Linlin Qi[1], Mateusz Kwiatkowski[2], Huihuang Chen[1], Lukas Hoermayer[1], Scott Sinclair[1], Minxia Zou[1], Charo I. del Genio[3], Martin F. Kubeš[4], Richard Napier[4], Krzysztof Jaworski[2], Jiří Friml[1,*]

Affiliations:

[1]Institute of Science and Technology Austria (ISTA) – 3400 Klosterneuburg (Austria).

[2]Department of Plant Physiology and Biotechnology, Nicolaus Copernicus University in Toruń – 87-100 Toruń (Poland).

[3]Centre for Fluid and Complex Systems, Coventry University – CV1 5FB Coventry (United Kingdom).

[4]School of Life Sciences, University of Warwick – CV4 7AL Coventry (United Kingdom).

[*] Correspondence to: jiri.friml@ist.ac.at

Abstract

Phytohormone auxin acts as major coordinative signal in plant development mediating transcriptional reprogramming by a well-established canonical signalling pathway: TIR1/AFB auxin receptors are F-box subunits of ubiquitin ligase complexes; in response to auxin they associate with Aux/IAA transcriptional repressors and by ubiquitination destine them for degradation. Here we identified adenylate cyclase (AC) activity as an additional functionality of TIR1/AFBs across land plants. Auxin together with Aux/IAAs stimulates cAMP production by TIR1/AFBs representing a novel signalling output from the TIR1/AFB-Aux/IAA co-receptor complex. Three separate mutations in the AC motif of the TIR1 C-terminal region, which all abolish the AC activity, render TIR1 ineffective in mediating gravitropism, auxin-induced root growth inhibition and partly compromise auxin-induced transcription. These discoveries highlight an importance of TIR1/AFB AC activity in auxin signalling. They also identify a unique phytohormone receptor cassette combining F-box and AC motifs, and new possibilities for cAMP as a second messenger in plants.

Main

Auxin is the major endogenous regulator of growth and development[1]. Earlier genetic screens based on auxin-induced root growth inhibition have identified major components of auxin signalling[2,3]. Further assisted by biochemical analysis, this established the core outline of the canonical auxin signalling pathway with TIR1/AFBs acting as auxin receptors. The sole proposed biochemical function of TIR1/AFBs is their action as F-box proteins, the subunits determining the substrate specificity of the SCF-type E3 ubiquitin ligase complex[4,5]. Auxin binding to the pocket of TIR1 increases the affinity between TIR1 and the Aux/IAA repressors,

promoting the ubiquitination and subsequent degradation of Aux/IAAs, thus releasing their repression on ARF-mediated transcription[5-8]. This nuclear mechanism explains how auxin can modulate transcription, and has stood the test of time for more than 15 years. However, several members of the TIR1/AFB family especially AFB1 are also present in cytosol[9], and recent accumulating observations suggest the existence of a non-transcriptional responses downstream of TIR1/AFBs[10,11]. Root growth inhibition strictly depends on functional TIR1/AFBs, but is very rapid and reversible[12]. It involves auxin-induced apoplast alkalinisation and membrane depolarization[13,14]. A member of the cyclic nucleotide-gated channel family (CNGC) CNGC14 is essential for auxin-induced cytosolic calcium (Ca^{2+}) transients and partially responsible for apoplast alkalinisation. These Ca^{2+} transients were originally proposed to be triggered by unknown cell surface auxin receptors[15], but later the CNGC14-Ca^{2+} pathway was placed downstream of TIR1/AFBs signalling in root hairs[16]. All of the above collectively suggests that TIR1/AFBs drive a non-transcriptional signalling activity, for which the underlying molecular mechanism remains a mystery. Hence, the molecular functions of TIR1/AFBs are still not fully elucidated.

Here we demonstrate that TIR1/AFB auxin receptors have adenylate cyclase (AC) activity, which is important for its physiological function in root growth regulation. This provides an unexpected twist to the mechanism of TIR1/AFB-mediated auxin signalling, and suggests cAMP as a second messenger in this key signalling mechanism in plants.

TIR1/AFBs auxin receptors have adenylate cyclase activity

The existence of an uncharacterized branch of TIR1/AFB signalling for root growth regulation[11] prompted us to search potential additional roles of TIR1/AFB auxin receptors by analysing their sequences.

Putative motifs for AC activities in plants have been identified by examining conserved sequences of reported AC proteins[17,18]. Screening the TIR1/AFBs protein sequences, we found a relatively conserved, possible AC motif in the unannotated C-terminal region (Fig. 1a) suggesting an AC activity of TIR1/AFB auxin receptors.

An *E. coli* complementation assay has been widely used to evaluate the AC activity of potential candidates, in which an AC-deficient strain (SP850) is complemented by genes of interest. Those possessing AC activity will produce cAMP, which can activate the lactose operon and change the colour of MacConkey agar to red[19]. We tested all 6 TIR1/AFBs with this assay, using a characterized AC (HpAC1) as a positive control[19]. Only AFB1 and AFB5 proteins can be detected by Western blot and those receptors also showed clear AC activity similar to HpAC1 (Extended Data Fig. 1a,b). Due to lack of detectable protein, the AC activity of the other 4 TIR1/AFBs could not be assessed. To further confirm AC activity, we purified GST-AFB5 protein from *E. coli* (Extended Data Fig. 2a), and performed an AC activity assay using the Enzyme Immunoassay Kit to detect cAMP. This revealed a clear AC activity of GST-AFB5, with a preference for Mn^{2+} as cofactor (Fig. 1b). To validate these results, we analysed the enzyme kinetics of GST-AFB5 by detection of cAMP with a more sensitive LC-MS/MS method. As shown in the LC-MS/MS spectrum, cAMP was reliably detected in the reaction system (Fig. 1c). The Michaelis-Menten kinetics identified a V_{max} = 10.45 fmol/min/µg and K_M = 0.675 mM for GST-AFB5 (Fig. 1d), which is comparable to other reported plant ACs[20-23]. Similarly, we also determined the AC enzyme kinetics for GST-AFB1 purified from *E. coli* (Extended Data Fig. 1c and Extended Data Fig. 2b). To test whether those members showing negative results in the *E. coli* complementation assay also have AC activity, we purified the His-GFP-FLAG-TIR1 protein from *Sf*9 insect cells (Extended Data Fig. 2c). We performed similar enzyme kinetics assay and identified a V_{max} = 7.462 fmol/min/µg and K_M = 0.644 mM for TIR1 (Fig. 1e and Extended Data Fig. 1d).

Comparison of orthologous sequences from the moss *Physcomitrella patents* revealed that the AC motif in the C-terminal of TIR1/AFBs is also conserved in this early diverging land plant (Extended Data Fig. 3a). We purified all 4 PpAFBs from *E.coli* (Extended Data Fig. 2d-g) and confirmed their AC activity (Extended Data Fig. 3b), showing that the TIR1/AFBs AC activity had already evolved in early ancestral land plants.

In summary, we demonstrated by three independent methods that TIR1, AFB1 and AFB5 possess AC activity, and given the conservation of the AC motif, it is likely that all 6 Arabidopsis TIR1/AFBs have AC activity. Moreover, the AC activity detected in the moss AFBs shows that it is a common feature also in the early diverging land plants.

A conserved C-terminal motif is responsible for the AC activity

The reported core AC motif [RKS]X[DE]X{9,11}[KR]X{1,3}[DE] contains 4 functionally assigned residues (Fig. 1a). [RKS] in position 1 allows hydrogen binding with adenine, [DE] in position 3 confers substrate specificity for ATP, [KR] stabilizes the transition state from ATP to cAMP, and the final [DE] residue is the cofactor Mg^{2+}/Mn^{2+} binding site[17]. Among the C-terminal AC motifs of TIR1/AFBs, the last 3 residues are highly conserved and strictly fit the original core motif, but the first residue is more relaxed, with only AFB2 and AFB3 having a perfectly matched motif. The demonstration of AC activity for TIR1, AFB1 and AFB5 extends the first residue from the original [RKS] to [RKSPY], so that all the 6 TIR1/AFBs have this extended AC motif in the C-terminal (Fig. 1a) suggesting that this motif is responsible for the AC activity.

To test this, we mutated separately the last 3 conserved residues in the C-terminal AC motif of AFB5 to alanine (m1, m2, m3 in Fig. 1a), and performed the *E. coli* complementation assay. The results showed that, while the mutated proteins expressed comparably to the wild-type

AFB5, all 3 mutated AFB5 variants lost their AC activity (Fig. 2a). To further confirm this, we purified the mutated GST-AFB5 from *E. coli* (Extended Data Fig. 2h) and performed the AC activity assay. Indeed, all mutated variants lost the AC activity except AFB5^{ACm2}, which maintained a very weak activity (Fig. 2b). Full-length TIR1 was unstable in the *E. coli* expression system, but we managed to purify an N-terminal deleted version (TIR1$^{\Delta NT}$) (Extended Data Fig. 2i), which still retains AC activity. We mutated the same 3 residues to alanine in the TIR1$^{\Delta NT}$ and purified them from *E. coli* (Extended Data Fig. 2j). Results from the AC activity assay clearly demonstrate that again all 3 mutations abolished the AC activity of TIR1$^{\Delta NT}$ (Fig. 2c).

To test whether these mutations interfere with auxin perception and the first step of the canonical pathway – the auxin induced TIR1/AFB interaction with Aux/IAAs, we introduced the same mutations into the full length TIR1. The pull-down reactions in presence of IAA with *in vitro* translated full length TIR1-HA and purified GST-IAA7 showed that while the ACm2 mutation abolished the interaction between TIR1^{ACm2} and IAA7, the ACm1 and ACm3 mutations did not have effects (Fig. 2d). This shows that the AC activity and Aux/IAA interaction capability can be uncoupled by ACm1 and ACm3 mutations in the AC motif.

Together, these results prove that the conserved C-terminal AC motif is responsible for the AC activity of TIR1/AFBs and can be mutated to selectively abolish this activity.

Auxin in conjunction with Aux/IAAs stimulate TIR1/AFB AC activity

Next, we tested whether auxin perception by TIR1/AFB has any effect on AC activity. According to the published crystal structure of TIR1, the C-terminus forms a cap structure, which closes the solenoid of leucine-rich repeats[8]. Spatially, the auxin binding pocket is located

close to the AC motif (Extended Data Fig. 4a), suggesting there may be mutual communication between the AC activity, auxin binding and auxin-triggered Aux/IAA interaction.

To gain additional insight into this issue, we docked the structure of ATP to the TIR1-IAA-Aux/IAA complex[8]. This shows that the orientation of ATP molecule, with the adenyl head close to the beginning of the AC domain (in magenta), the sugar moiety in direct contact with E554 (ACm1 in Fig. 1a), and the phosphate groups next to a positively charged residue R555, fits plausibly into the structure of the TIR1-IAA-Aux/IAA complex. However, the remaining half of the AC motif including the two amino acids we mutated before R566 (ACm2) and D568 (ACm3) is on the other side of the TIR1 surface without a direct predicted contact with the docked ATP (Fig. 3a and Extended Data Fig. 4b). It is possible that the crystalized structure does not reflect the genuine structure *in planta*, or that ATP binding causes conformational change. Importantly, V84 from the Aux/IAA degron constrains space available to ATP, possibly reducing its mobility and thus increasing the reaction efficiency (Fig. 3a). This structural perspective suggests that the auxin-triggered association between Aux/IAAs and TIR/AFBs may enhance their AC activity.

To test this, we purified AFB5, along with the IAA7 and IAA17 co-receptors from *E. coli* with GST tags cleaved (Extended Data Fig. 2k-m) and performed *in vitro* AC activity assays for AFB5 in the presence of 10 μM IAA, IAA7 or IAA17, and their combinations. The results showed that IAA or IAA7/17 alone did not have any significant effect on the AFB5 AC activity. However, IAA together with IAA7 or IAA17 significantly enhanced the AC activity, with IAA7 showing a stronger effect than IAA17 (Extended Data Fig. 5). To confirm this observation, we did similar experiment with His-GFP-FLAG-TIR1 protein purified from *Sf9* insect cells. Again, significant increase in TIR1 AC activity was observed in the presence of IAA together with IAA7 or IAA17 (Fig. 3b). These results show that the IAA-induced assembly of the TIR1-Aux/IAA complex enhances the AC activity.

Next, we tested whether stimulation of TIR1/AFB AC activity can be detected *in planta*. We treated Col-0 seedlings with 100 nM IAA and harvested roots at different time points to measure cAMP level using LC-MS/MS. Indeed, after an initial slight depletion of cAMP, IAA treatment led to a steady increase of cAMP levels after 1 h (Fig. 3c). Whilst only the difference at 6 h is statistically significant, this dynamic trend was reproducible in multiple repetitions. Considering that TIR1/AFBs are not the only ACs in *Arabidopsis* and the list of AC enzymes is growing continuously[17,18], and that cAMP signalling is likely highly compartmentalized[24] leading to a very localized increase of cAMP levels around the TIR1/AFBs receptors themselves, the activation effect will be predictably underestimated by measuring entire root cAMP content. Hence, the detected differences, whilst small in whole root tissue, are likely physiologically relevant. Notably, the increase of cAMP levels after auxin treatment was completely abolished in *tir1-1 afb2-1 afb3-1* (*tir* triple) mutant, and even values for both Mock and IAA in *tir* triple were slightly lower comparing to the Mock value of Col-0 (Fig. 3d). Collectively, these data indicate that auxin treatment increases cAMP level in roots through TIR1/AFBs.

Collectively, these data show that the auxin-induced interaction between TIR1/AFBs and Aux/IAAs stimulates the AC activity consistent with auxin-triggered cAMP increase in roots. This represents a novel molecular output of TIR1/AFBs, distinct from their E3 ligase activity.

TIR1 AC activity is crucial for root growth inhibition and root gravitropism

To evaluate the importance of the AC activity to the physiological function of TIR1 *in planta*, we tested the ability of TIR1$^{ACm1\text{-}3}$ protein variants to mediate root growth regulation by introducing the *pTIR1::TIR1*$^{ACm1\text{-}3}$ constructs into *tir1-1 afb2-3* double mutant. As shown before[25], root growth was strongly inhibited when Col-0 seedlings were grown on plates

containing 100 nM IAA, while *tir1-1 afb2-3* was completely resistant under these conditions. The *pTIR1::TIR1* almost fully complemented this mutant phenotype, whereas all 3 mutated *pTIR1::TIR1*$^{ACm1-3}$ variants showed compromised complementation (Fig. 4a,b). Notably, the TIR1^{ACm2} mutation, which also abolishes the interaction with Aux/IAAs (see Fig. 2d), rendered TIR1 completely non-functional. Overall, this shows that AC activity is crucial for the TIR1-mediated root growth inhibition by auxin.

To further confirm this notion, we used the synthetic biology tool, the engineered cvxIAA-ccvTIR1 pair system[26]. As illustrated (Fig. 4c), natural IAA can only bind TIR1 to trigger root growth inhibition but not the ccvTIR1 with the engineered auxin binding site and vice versa, the auxin analogue cvxIAA binds and activates only ccvTIR1 but not the TIR1 or AFBs. Therefore, *pTIR1::TIR1*, *pTIR1::ccvTIR1* and the 3 corresponding mutated *pTIR1::ccvTIR1*$^{ACm1-3}$ constructs were generated and transformed into the *tir1-1 afb2-3* background. Consistent to the previous reports[26], cvxIAA (500 nM) cannot trigger root growth inhibition in the absence of the engineered ccvTIR1, but triggers strong root growth inhibition in the *ccvTIR1 t*ransgenic plants. Again *ccvTIR*^{ACm2} showed a complete resistance (Fig. 4d) in line with its additional inability to interact with Aux/IAAs (see Fig. 2d), whereas in *ccvTIR*^{ACm1} as well as *ccvTIR*^{ACm3} lines also almost no root growth inhibition was observed (Fig. 4d). This confirms that TIR1 AC activity is essential for TIR1's role in mediating root growth inhibition by auxin.

Auxin effect on root growth underlies positive root gravitropism[27]. To test whether TIR1 AC activity is also required for root gravitropism, we analysed the dynamics of gravitropic root bending angle in the *pTIR1::TIR1* and *pTIR1::TIR1*$^{ACm1/3}$ complemented lines. *tir1-1 afb2-3* has clear defects in root gravitropic response comparing to Col-0. *pTIR1::TIR1* largely complemented the gravitropic defects of *tir1-1 afb2-3*, while *TIR1*^{ACm1} and *TIR1*^{ACm3} showed

only very slight complementation (Fig. 4e). This result proves that AC activity of TIR1 is also required for root gravitropism.

These genetic experiments collectively show that AC activity is crucial for TIR1 function in auxin-induced root growth inhibition and root gravitropism *in planta*.

TIR1 AC activity is not essential for rapid auxin effects in roots

To understand the temporal dynamics of the importance of AC activity for root growth regulation by auxin, we evaluated the root growth kinetics of *pTIR1::ccvTIR1* and *pTIR1::ccvTIR1*^{ACm1} lines using vRootchip in combination with vertical microscopy[12,13]. cvxIAA application gradually inhibited root growth in both lines, but no significant difference was observed between them within the 1st hour (Extended Data Fig. 6a). Then we followed the root growth dynamics with a vertical scanner finding that the resistance of *pTIR1::ccvTIR1*^{ACm1} to cvxIAA-induced root growth inhibition occurs only after 1 h (Extended Data Fig. 6b) correlating with the dynamics of the auxin-induced increase of cAMP level in root (see Fig. 3c). This suggests that TIR1 AC activity is required for root growth regulation only at later stages.

It has been demonstrated previously that auxin-induced rapid root growth inhibition is closely related to Ca^{2+} signalling and apoplast alkalinisation[13,15]. To clarify whether TIR1 AC activity is required for these rapid non-transcriptional responses, we monitored the cytosolic Ca^{2+} spikes and apoplast alkalinisation in the AC motif-mutated *TIR1* transgenic lines. cvxIAA triggers similar cytosolic Ca^{2+} increase in *ccvTIR1* and *ccvTIR1*^{ACm1} lines within 1 min, and there is also no significant difference for IAA-induced apoplastic pH increase in *TIR1* and *TIR1*^{ACm1} lines (Extended Data Fig. 7a,b).

Together, these observations indicate that TIR1 AC activity, despite being crucial for the sustained auxin-induced root growth inhibition, is not essential for rapid auxin effect on root growth and associated rapid apoplast alkalinisation and Ca^{2+} transients.

TIR1 AC activity contributes to the auxin-induced transcriptional regulation

Since the TIR1 AC activity seems to be important only for a long-term auxin effects on root growth and gravitropism, which are likely involving transcriptional regulation, we tested auxin effect on transcription of selected auxin responsive genes using quantitative real-time PCR (qRT-PCR). Consistent with previous results[26], cvxIAA specifically activates the transcription of the selected auxin-responsive genes including *GH3.3*, *GH3.5*, *IAA5*, *IAA19* and *LBD29* in *ccvTIR1*, but not in control *TIR1* line. Indeed, the transcriptional upregulation of these genes is notably reduced in *ccvTIR*^{ACm1} (Fig. 4f-j), suggesting that TIR1 AC activity also contributes to auxin-induced transcriptional regulation.

Conclusions

The current framework of canonical auxin signalling relies on TIR1/AFB auxin receptors acting as F-box proteins, which form a functional SCF-type E3 ubiquitin ligase together with other subunits[4-7]. Here we show that TIR1/AFBs have an additional, adenylate cyclase activity with the responsible AC motif in the unannotated C-terminal region (Fig. 1, Fig. 2 and Extended Data Fig. 3). As shown in Arabidopsis and moss, presumably, all TIR1/AFBs across land plants have this activity. The N-terminal localized F-box and C-terminal AC motif are spatially separated, suggesting that the ubiquitin ligase and AC activities are independent.

Hence, TIR1/AFBs represent a unique type of hormone receptor combining F-box and AC motifs.

Auxin binding and AC activity sites are in spatial proximity within the TIR1 protein structure (Extended Data Fig. 4a). Docking of ATP to TIR1 structure shows that V84 from the Aux/IAA degron works like a latch to constrain the space available to ATP, suggesting it may reduce its mobility and thus enhance the AC reaction efficiency (Fig. 3a). Indeed, auxin together with the Aux/IAA co-receptors enhances the AC activity *in vitro* (Fig. 3b and Extended Data Fig. 5). Moreover, cAMP content in roots starts to increase after auxin treatment (Fig. 3c), and such increase is completely dependent on TIR1/AFBs auxin receptors (Fig. 3d). Thus, auxin-activated cAMP production, in addition to Aux/IAA degradation, represents a previously unsuspected signalling output from the TIR1/AFB-Aux/IAA co-receptor complex. This implies the product of the AC activity - cAMP - as a second messenger in auxin signalling.

Accumulating evidence points to the existence of an elusive non-transcriptional branch of TIR1/AFB auxin signalling mediating rapid cellular processes such as cytosolic Ca^{2+} spikes, membrane depolarization and apoplast alkanization[13,14,16], all linked to root growth inhibition[12]. Our expectation was that the newly identified AC activity of TIR1/AFBs would mediate these rapid effects. Nonetheless, despite abolishing AC activity in $TIR1^{ACm}$ variants renders them incapable of mediating auxin-induced root growth inhibition (Fig. 4a-d), this effect does not extend to the very rapid responses (Extended Data Fig. 7a,b). The $ccvTIR1^{ACm1}$-based root growth resistance to cvxIAA (Extended Data Fig. 6a,b) as well as TIR1/AFB-mediated cAMP production (Fig. 3c) have dynamics slower than 1 hour. Furthermore, mutating TIR1 AC activity also compromises auxin-induced transcription of selected genes (Fig. 4f-j). These observations suggest that AC activity of TIR1/AFB receptors contributes to the canonical, transcriptional pathway and an additional mechanism is required for a very rapid response.

Historically, cNMPs are highly important and well established second messengers in mammalian models[28]. Comparably, cNMP research in plants is progressing slowly[17,29]. Nonetheless, the list of proteins with detected AC activity *in vitro* has been steadily growing[17,18,20-23] as for proteins with GC activity, which includes such prominent candidates as the brassinosteroid and phytosulfokines receptors[18,30,31]. Generally, the characterized plant ACs/GCs have lower activities than their animal counterparts, and accordingly average cNMP levels in plant tissues are also lower[17,23]. Therefore, *in planta* relevance of the AC and GC activities remains unclear and controversial, also due to the lack of genetic support and clearly defined downstream effectors. Thus, the AC activity of TIR1/AFB auxin receptors and its key importance for root growth regulation brings new prominence to the role of ACs in plants and an incentive to rejuvenate cNMP signalling research in plant biology.

References

1 Friml, J. Fourteen stations of auxin. *Cold Spring Harb. Perspect. Biol.* **14**, a039859 (2021).

2 Parry, G. & Estelle, M. Auxin receptors: a new role for F-box proteins. *Curr. Opin. Cell Biol.* **18**, 152-156 (2006).

3 Quint, M. & Gray, W. M. Auxin signaling. *Curr. Opin. Plant Biol.* **9**, 448-453 (2006).

4 Gray, W. M. et al. Identification of an SCF ubiquitin-ligase complex required for auxin response in Arabidopsis thaliana. *Genes Dev.* **13**, 1678-1691 (1999).

5 Gray, W. M., Kepinski, S., Rouse, D., Leyser, O. & Estelle, M. Auxin regulates SCF^{TIR1}-dependent degradation of AUX/IAA proteins. *Nature* **414**, 271-276 (2001).

6 Dharmasiri, N., Dharmasiri, S. & Estelle, M. The F-box protein TIR1 is an auxin receptor. *Nature* **435**, 441-445 (2005).

7 Kepinski, S. & Leyser, O. The Arabidopsis F-box protein TIR1 is an auxin receptor. *Nature* **435**, 446-451 (2005).

8 Tan, X. et al. Mechanism of auxin perception by the TIR1 ubiquitin ligase. *Nature* **446**, 640-645 (2007).

9 Prigge, M. J. et al. Genetic analysis of the Arabidopsis TIR1/AFB auxin receptors reveals both overlapping and specialized functions. *eLife* **9**, e54740 (2020).

10 Kubes, M. & Napier, R. Non-canonical auxin signalling: fast and curious. *J. Exp. Bot.* **70**, 2609-2614 (2019).

11 Gallei, M., Luschnig, C. & Friml, J. Auxin signalling in growth: Schrodinger's cat out of the bag. *Curr. Opin. Plant Biol.* **53**, 43-49 (2020).

12 Fendrych, M. et al. Rapid and reversible root growth inhibition by TIR1 auxin signalling. *Nat. Plants* **4**, 453-459 (2018).

13 Li L. et al. Cell surface and intracellular auxin signalling for H^+ fluxes in root growth. *Nature* **599**, 273-277 (2021).

14 Serre, N. B. C. et al. AFB1 controls rapid auxin signalling through membrane depolarization in Arabidopsis thaliana root. *Nat. Plants* **7**, 1229-1238 (2021).

15 Shih, H. W., DePew, C. L., Miller, N. D. & Monshausen, G. B. The cyclic nucleotide-gated channel CNGC14 regulates root gravitropism in Arabidopsis thaliana. *Curr. Biol.* **25**, 3119-3125 (2015).

16 Dindas, J. et al. AUX1-mediated root hair auxin influx governs $SCF^{TIR1/AFB}$-type Ca^{2+} signaling. *Nat. Commun.* **9**, 1174 (2018).

17 Gehring, C. Adenyl cyclases and cAMP in plant signaling - past and present. *Cell Commun. Signal.* **8**, 15 (2010).

18 Wong, A., Gehring, C. & Irving, H. R. Conserved functional motifs and homology modeling to predict hidden moonlighting functional sites. *Front. Bioeng. Biotechnol.* **3**, 82 (2015).

19 Swiezawska, B. et al. Molecular cloning and characterization of a novel adenylyl cyclase gene, HpAC1, involved in stress signaling in Hippeastrum x hybridum. *Plant Physiol. Biochem.* **80**, 41-52 (2014).

20 Al-Younis, I., Wong, A. & Gehring, C. The Arabidopsis thaliana K(+)-uptake permease 7 (AtKUP7) contains a functional cytosolic adenylate cyclase catalytic centre. *FEBS Lett.* **589**, 3848-3852 (2015).

21 Al-Younis, I. et al. The Arabidopsis thaliana K(+)-uptake permease 5 (AtKUP5) contains a functional cytosolic adenylate cyclase essential for K(+) transport. *Front. Plant Sci.* **9**, 1645 (2018).

22 Chatukuta, P. et al. An Arabidopsis clathrin assembly protein with a predicted role in plant defense can function as an adenylate cyclase. *Biomolecules* **8**, 15 (2018).

23 Bianchet, C. et al. An Arabidopsis thaliana leucine-rich repeat protein harbors an adenylyl cyclase catalytic center and affects responses to pathogens. *J. Plant Physiol.* **232**, 12-22 (2019).

24 Johnstone, T. B., Agarwal, S. R., Harvey, R. D. & Ostrom, R. S. cAMP signaling compartmentation: adenylyl cyclases as anchors of dynamic signaling complexes. *Mol. Pharmacol.* **93**, 270-276 (2018).

25 Parry, G. et al. Complex regulation of the TIR1/AFB family of auxin receptors. *PNAS* **106**, 22540-22545 (2009).

26 Uchida, N. et al. Chemical hijacking of auxin signaling with an engineered auxin-TIR1 pair. *Nat. Chem. Biol.* **14**, 299-305 (2018).

27 Li, L., Gallei, M. & Friml, J. Bending to auxin: fast acid growth for tropisms. *Trends Plant Sci.* **27**, 440-449 (2022).

28 Beavo, J. A. & Brunton, L. L. Cyclic nucleotide research -- still expanding after half a century. *Nat. Rev. Mol. Cell Biol.* **3**, 710-718 (2002).

29 Trewavas, A. J. Plant cyclic AMP comes in from the cold. *Nature* **390**, 657-658 (1997).

30 Kwezi, L. et al. The phytosulfokine (PSK) receptor is capable of guanylate cyclase activity and enabling cyclic GMP-dependent signaling in plants. *J. Biol. Chem.* **286**, 22580-22588 (2011).

31 Wheeler, J. I. et al. The brassinosteroid receptor BRI1 can generate cGMP enabling cGMP-dependent downstream signaling. *Plant J.* **91**, 590-600 (2017).

Figure legends

Figure 1. TIR1/AFB auxin receptors have adenylate cyclase activity

a, Alignment of the C-terminal protein sequences of TIR1/AFBs with the conserved AC motif. LRR, leucine-rich repeat. The residues m1-m3 indicate the conserved key amino acids, which were mutated to alanine to disrupt the AC activity (shown in Fig. 2).

b-d, *in vitro* AC activity of GST-AFB5 purified from *E.coli*. AC activity assay in the presence of 2 different co-factors, followed by cAMP quantification by EIA (Enzyme ImmunoAssay) kit. The values shown were blanked against the background signals from the corresponding GST samples (**b**). Typical LC-MS/MS spectrum showing cAMP detection in the AC reaction with the characteristic peak used for quantification (**c**). Michaelis-Menten kinetics for the AC activity quantified by LC-MS/MS. S, substrate; V, velocity (**d**). For each data point, means ± SD from 3 biological replicates are shown.

e, *in vitro* AC activity of His-GFP-FLAG-TIR1 purified from *Sf9* insect cells. Michaelis-Menten kinetics giving results similar to GST-AFB5 (shown in d).

Figure 2. C-terminal AC motif is responsible for the TIR1/AFB AC activity

a-b, C-terminal AC motif is essential for the AFB5 AC activity. The AC deficient *E. coli* strain SP850 was complemented by the indicated constructs. The red colour of the MacConkey agar indicates the presence of AC activity. The empty vector *pGEX-4T-1* was used as negative control. Western blot confirms similar expression levels of endogenous and mutated AFB5 proteins. Ponceau staining of the membrane was used as the loading control (**a**). *in vitro* AC activity assay for the purified GST-AFB5 and 3 mutated variants, followed by the cAMP

386 quantification using LC-MS/MS. V, velocity. The values shown are means ± SD from 3
387 biological replicates (**b**).

388 **c**, C-terminal AC motif is essential for the AC activity of TIR1$^{\Delta NT}$. GST-TIR1$^{\Delta NT}$ and 3
389 mutated variants were purified from *E. coli*. An *in vitro* AC activity assay was performed
390 followed by cAMP quantification using LC-MS/MS. V, velocity. The values shown are means
391 ± SD from 3 biological replicates.

392 **d**, Pull-down results showing differential effects of TIR1^{ACm} mutations on the IAA-induced
393 TIR1-Aux/IAA interaction. Wild-type and the 3 mutated TIR1 variants were translated *in vitro*
394 using wheat germ extracts, and were then used for pull-down assays with purified GST-IAA7,
395 in the presence or absence of 10 μM IAA as indicated.

396

397 **Figure 3. Auxin perception enhances the TIR1/AFBs AC activity**

398 **a**, Docking of ATP on the surface of TIR1-IAA-Aux/IAA complex. The beginning of the AC
399 center was labelled in magenta. Amino acids presumably important for the AC activity were
400 labelled either in red (acidic), or in blue (basic). E554 is the site for m1 (as in Fig. 1a). Note
401 that V84 from the Aux/IAA degron restricts the space available to ATP.

402 **b**, Auxin together with Aux/IAA stimulates the TIR1 AC activity. *in vitro* AC activity assay
403 with His-GFP-FLAG-TIR1 (5 μg) in the presence of 10 μM IAA, IAA7 (3 μg), IAA17 (3 μg)
404 and the indicated combinations, followed by cAMP quantification using LC-MS/MS. V,
405 velocity. One-way ANOVA. n = 3. *** $p \leqslant 0.001$; **** $p \leqslant 0.0001$.

406 **c**, Auxin treatment increases cAMP content in root tissues . Five-days-old Col-0 seedlings were
407 treated with 100 nM IAA. Root tissues were harvested for cAMP quantification by LC-MS/MS.
408 One-way ANOVA. n = 3. * $p \leqslant 0.05$.

d, Auxin-induced increase of cAMP levels in roots is dependent on TIR1/AFBs. Five-days-old Col-0 or *tir* triple seedlings were treated with 100 nM IAA for 6 h. Root tissues were collected for cAMP measurement by LC-MS/MS. One-way ANOVA. n = 3. * $p \leqslant 0.05$. ns, not significant.

Figure 4. TIR1 AC activity contributes to auxin-induced root growth inhibition and transcriptional responses

a-b, AC motif mutations compromise TIR1 function in mediating IAA-induced root growth inhibition. *pTIR1::TIR1* and the similar constructs containing the 3 AC motif mutations were transformed into *tir1-1 afb2-3*. Representative examples of 6-days-old seedlings of different genotypes grown on Mock or 100 nM IAA containing medium. Bar = 10 mm (**a**). Quantification of the root length in (a). n = 30 (**b**).

c, Simplified scheme showing the principles of the engineered cvxIAA/ccvTIR1 system.

d, C-terminal AC motif is crucial for cvxIAA-triggered root growth inhibition in *ccvTIR1* line. *pTIR1::TIR1*, *pTIR1::ccvTIR1*, and the 3 similar constructs containing the AC motif mutations (see Fig. 1a) were transformed into *tir1-1 afb2-3*. Root length of the 6-days-old seedlings with different genotypes grown on Mock or 500 nM cvxIAA containing medium were measured. n = 30.

e, AC activity is required for TIR1 function in root gravitropism. Five-days-old seedlings of the indicated genotypes were transferred to new plates. The plates were rotated 90 degree before images were captured every 30 min. Root bending angle was measured to monitor the gravitropic response. n = 10.

f-j, AC activity contributes to auxin-induced genes expression. Five-days-old seedlings were either Mock-treated or treated with liquid medium containing 200 nM cvxIAA for 3 h. Seedlings were harvested for RNA extraction and qRT-PCR. Shown are the relative expression values normalized to the internal control *PP2AA3*, from 3 or 4 biological replicates.

Methods

Plant materials and growth conditions

All the *Arabidopsis* mutants and transgenic lines used in this study are in Columbia-0 (Col-0) background. The *tir1-1 afb2-3* mutant was shared by Keiko U. Torii[26]. The *tir1-1 afb2-1 afb3-1*[32], and the calcium sensor GCaMP3[33] have been described previously. To generate the complementation lines *pTIR1::TIR1*, *pTIR1::TIR1*^{ACm1}, *pTIR1::TIR1*^{ACm2} and *pTIR1::TIR1*^{ACm3} in *tir1-1 afb2-3*, *TIR1* promoter sequence was amplified from genomic DNA and cloned into pDONR P4-P1r, and the *TIR1* CDS (coding domain sequence) was cloned into pDONR221. To mutate the AC motif in TIR1, Phusion Site-Directed Mutagenesis Kit (Thermo Fisher, F541) was used, with the plasmid of *TIR1* in pDONR221 as the template. The resulting entry clones were recombined into the destination vector pB7m24GW to get the final expression vectors. The constructs *pTIR1::ccvTIR1* and the mutated versions *pTIR1::ccvTIR1*^{ACm1}, *pTIR1::ccvTIR1*^{ACm2} and *pTIR1::ccvTIR1*^{ACm3} were generated in a similar way. F79G mutation was used to generate the engineered ccvTIR1 according to the previous report[26]. All the primers used for plasmid construction are listed in Extended Data Table 1. The final expression constructs were transformed into the *Agrobacterium tumefaciens* strain GV3101 by electroporation. Floral dip method was used to transform the *Arabidopsis* plants.

Seeds were surface-sterilized by chlorine gas, sown on half-strength Murashige and Skoog (½ MS) medium supplemented with 1% (w/v) sucrose and 0.8% (w/v) phyto agar (pH 5.9), stratified in the dark at 4°C for 2 days and then grown vertically at 21°C with a long-day photoperiod (16 h light/8 h dark). Light sources used were Philips GreenPower LED production modules [in deep red (660 nm)/far red (720 nm)/blue (455 nm) combination, Philips], with a photon density of 140.4 μmol/m^2/s ± 3%[13].

Root growth assays

Seeds were directly sown on plates containing different treatment medium. Six-days-old seedlings were scanned with a horizontal scanner (Epson Perfection V800 Photo) to acquire images. Root length was measured using the segmentation plugin Simple Neurite Tracer in Image J[34]. To track the root growth dynamics, a vertical scanner growth assay was performed as previously described[13]. Simply, five-days-old seedlings were transferred to petri dishes filled with treatment medium. The petri dishes were fixed with a mold into a vertically mounted scanner (Epson Perfection v.370), so that root can grow vertically during imaging. Roots were imaged automatically every 30 min using the AutoIT script described previously[35]. The resulting image series were registered using StackReg and root growth rate was measured using the Manual Tracking plugin in ImageJ. To evaluate root growth in a high temporal resolution, the microfluidic vRootchip was used as previously described[12,13]. For root gravitropism assay, it was done in a similar way with the vertical scanner growth assay, except the plates with seedlings were rotated 90 degree to give a gravi-stimulation when placed onto the vertical scanner. Root bending angles were measured based on the output from the Manual Tracking plugin in ImageJ.

E. coli complementation assay

The *E. coli* SP850 strain (lam-, el4-, relA1, spoT1, cyaA1400(:kan), thi-1), deficient in adenylate cyclase, was originally obtained from the *E. coli* Genetic Stock Center (Yale University, New Haven, USA) (accession number 7200) and shared by Krzysztof Jaworski. The positive control HpAC1[19], and the potential candidate genes TIR1/AFBs were cloned into pGEX-4T-1. The primers and restriction sites used are listed in Extended Data Table 1. The overnight SP850 cultures (10 μL) containing the indicated constructs were streaked onto

MacConkey agar with ampicillin (100 μg/ml) and IPTG (100 μM). The plates were incubated at 37ºC for 12 h, and the images were obtained.

Western blot

The overnight SP850 cultures containing different constructs were inoculated at the dilution of 1:100 into LB medium with ampicillin (100 μg/ml) and IPTG (100 μM), and were then cultured at 37ºC for another 6 h for protein induction. Cells were pelleted from equal volume of the induced cultures (1 mL), directly lysed in Laemmli Sample Buffer (Biorad, 1610747), and denatured at 95°C for 5 min. Supernatants were loaded into 10% precast gel (Mini-Protean® TGX™, Bio-Rad). After separation, proteins were transferred to PVDF membranes by electroblotting (Trans-blot® Turbo™, Bio-Rad). The immunoblotting was performed following the standard procedure with the anti-GST-tag, HRP-conjugated monoclonal antibody (Agrisera, AS18 4188) at the dilution of 1:2000. Chemiluminescence signal was detected with Bio-Rad ChemiDoc™ MP Imager. Ponceau staining of the membrane was used to show the equal loading.

Protein purification

Gene sequences for protein expression in *E. coli* were cloned into pGEX-4T-1 vector using the primers listed in Extended Data Table 1. The resulting plasmids were introduced into the BL21 competent cells (NEB, C2530H) in order to produce the fusion proteins with GST (glutathione-S-transferase) affinity tag. The transformants were grown in LB medium (500 mL) containing ampicillin (100 μg/mL) and 2% glucose at 37°C. Fusion protein expression was induced by adding IPTG (isopropyl-ß-D-thiogalactopyranoside) to a final concentration of 0.5 mM at OD600 = 0.6 and incubating the culture at 18°C for 4 h. The bacteria were harvested by

centrifugation and the pellet was suspended in lysis buffer (50 mM Tris-HCl pH 8.0, 150 mM NaCl, 5 mM EDTA, 5 mM EGTA, 1% (v/v) Triton X-100, 1 mM PMSF, 0.2 mg/mL lysozyme) and disrupted by sonication. The cell extract was centrifuged at 18,000 × g for 35 min and the supernatant was loaded onto a glutathione-Sepharose 4B beads (GE Healthcare). Afterward, the column was washed multiple times with buffer containing 50 mM Tris-HCl (pH 8.0), 150 mM NaCl and the GST fusion protein was eluted with 10 mM glutathione in 50 mM Tris-HCl (pH 9.0). The homogeneity and purity of eluted protein fraction was analyzed by SDS–PAGE electrophoresis (8% gel) with the Coomassie Blue gel staining.

To remove GST affinity tag by thrombin cleavage, the cell extract after centrifugation at 18,000 × g for 35 min was loaded onto a GSTrap™ FF column using an ÄKTA start system (GE Healthcare). After washing the column with binding buffer (140 mM NaCl, 2.7 mM KCl, 10 mM Na_2HPO_4, 1.8 mM KH_2PO_4, pH 7.3), 20 U of thrombin (Sigma, 604980) was dissolved in binding buffer and applied to the column via 1 mL loop. The column was sealed and incubated at 22°C for 6 h. After incubation, the HiTrap™ Benzamidine FF column (Sigma, GE17-5143-02) was placed in series directly after the GSTrap™ FF column for thrombin binding. The columns were washed with binding buffer and the pure proteins were collected in 0.5 mL fractions. The homogeneity and purity of eluted protein fraction was analyzed by SDS–PAGE electrophoresis (8% gel) with the Coomassie Blue gel staining.

To purify TIR1 full-length protein from *Sf9* insect cells. A vector was constructed to co-express His-GFP-(TEV)-FLAG-TIR1 and His-(TEV)-ASK1. Generation of recombinant virus and infection were all done as previously described[36,37]. To purify TIR1 protein, the frozen cell pellets were thawed and resuspended in lysis buffer containing equal volumes of CytoBuster™ Protein Extraction Reagent (Millipore, 71009-3) and buffer A (20 mM Tris-HCl pH 7.4, 200 mM NaCl, 1 mM EDTA, Protease Inhibitor Cocktail (Sigma) and 1 mM TCEP). The lysis solution was mixed by rolling at 4°C for 45 min. Lysate was then disrupted by sonication and

centrifuged at 20,000 × g for 20 min. The supernatant was collected and filtered through a 0.45 μm and 0.2 μm filters (Merck). All subsequent steps took place in the cold room at 4°C. Before applying the sample to the nickel metal affinity chromatography column, cOmplete His-Tag Purification Resin (Roche) was washed and equilibrated with buffer A for 1 h. Filtrate was then loaded onto the conditioned column and the resin was washed with 5 volumes of buffer A. Then the resin was washed with 5 volumes of buffer A (without TCEP) containing 10 mM imidazole. Fusion protein was eluted with buffer B (buffer A, 250 mM imidazole). Eluted proteins were then loaded onto Pierce™ Anti-FLAG Affinity Resin (Thermo Scientific, A36801), previously equilibrated with buffer A, to remove free ASK1 protein. The column was placed on a rotor and mixed for 1 h. Resin was then washed 3x with 5 bed volumes of PBS (pH 7.2) and 1x with 5 bed volumes of purified water. Fusion TIR1 protein was eluted with 2 mL of 1.5 mg/mL Pierce™ 3x DYKDDDDK peptide (Thermo Scientific, A36805), according to manufacturer instructions. FLAG peptide was then removed by desalting using Zeba™ Spin Desalting Columns (Thermo Scientific, 89891), according to manufacturer instructions. The homogeneity and purity of protein was analyzed by SDS–PAGE electrophoresis (8% gel) with the Coomassie Blue gel staining.

in vitro **AC activity assay**

in vitro AC activity of the purified proteins was determined by evaluating the rate of cAMP formation. The reaction mixture contained: 10 mM Tris-HCl buffer (pH 7.6), 1 mM $MgCl_2$ and/or 1 mM $MnCl_2$, 1 mM IBMX (3-isobutyl-1-methylxanthine), 1 mM ATP, 1 mM DTT and 5 μg of the protein in a final volume of 100 μL. To investigate the effects of IAA on the AC activity of AFB5, 10 μM IAA was added to the reaction mixture along with 5 μg of IAA7 or IAA17. Samples were then incubated at 30°C for 25 min. The enzyme reaction was terminated

by incubation at 100 °C for 10 min and the samples were centrifuged at 16,100 × g for 10 min. The cAMP level after the reaction was quantified using either the Amersham cAMP Biotrak Enzymeimmunoassay system (GE, RPN225) or LC-MS/MS. For cAMP measurement with enzyme immunoassay, the acetylation assay was performed following the standard procedures of Protocol 2 in the product booklet. The AC reaction product was diluted 10 fold with assay buffer during the assay.

Root cAMP extraction and quantification

Five-days-old Col-0 or *tir* triple seedlings grown in 12 cm × 12 cm square plates were sprayed with 20 mL of ½ MS liquid medium without or with 100 nM IAA per plate. At the indicated time points, root tissues were harvested and immediately frozen in liquid nitrogen. Isolation of cAMP from root tissues was carried out according to the published method[38], with minor changes. Frozen roots were homogenized manually with a pre-cooled mortar and pestle with liquid nitrogen. The grounded powder was weighed and about 100 mg of sample was transferred to a 2 mL Eppendorf tube and 600 µL of 4% acetic acid together with 10 µL of IBMX (1 mM) were added. Sample was vortexed for 30 s and centrifuged for 5 min at 5000 × g at 4 °C. The supernatant was collected, 1200 µL of acetonitrile was added and the sample was centrifuged again for 5 min at 5000 × g at 4°C. The supernatant was transferred to a 15 mL Falcon® tube and 200 µL of 5/95 100 mM ammonium formate/acetonitrile buffer, 200 µL of water and 2 mL of acetonitrile were added. Subsequently the sample was vortexed for 1 min and centrifuged for 5 min at 2000 × g. The supernatant was then transferred to the silica Discovery® DSC-18 SPE 1 mL Tube (Sigma, St. Louis MO, USA), that was first conditioned with 2.5 mL of water under vacuum conditions and equilibrated with 2.5 mL of 5/95 100 mM ammonium formate/acetonitrile. The supernatant was slowly drawn through the SPE cartridge

by vacuum conditions. After sample loading the SPE tube was washed with 1 mL of 10/90 water/acetonitrile and the analyte was eluted with 0.5 mL of water followed by filtering (0.2 µm, Merck, Ireland). The samples were lyophilized, reconstituted in 50 µL of water and 5 µL was injected into the LC–MS/MS system for analysis.

LC-MS/MS (Liquid chromatography-tandem mass spectrometry) analysis

LC-MS/MS experiments were performed using the Nexera UHPLC and LCMS-8045 integrated system (Shimadzu Corporation). The ionization source parameters were optimized in positive ESI mode using pure cAMP dissolved in HPLC-grade water (Sigma). Samples were separated at 40°C using a XSelect CSH Phenyl-Hexyl column (100 x 2.1 mm, 3.5 µm, Waters). An isocratic flow of 90% solvent A (0.05% (v/v) formic acid with 5 mM ammonium formate) and 10% solvent B (100% (v/v) acetonitryle) was applied over 5 min, followed by washing and conditioning of the column, with a flow rate of 0.4 mL/min. The interface voltage was set at 4.0 kV for positive (ES+) electrospray. Data acquisition and analysis were made with the LabSolutions workstation for LCMS-8045.

Pull-down assays

The coding sequence of TIR1-HA was cloned into pF3A WG (BYDV) Flexi® Vector (Promega, L5671) for *in vitro* translation. Similar TIR1^{ACms}-HA constructs were obtained using Phusion Site-Directed Mutagenesis Kit (Thermo Fisher, F541). 3 µg of plasmids were used for each 50 µL of *in vitro* translation reaction using TnT® SP6 High-Yield Wheat Germ Protein Expression System (Promega, L3260). For pull-down, 20 µL of *in vitro* translated proteins were incubated with 5 µg of GST-IAA7 purified from *E. coli*, in the presence or absence of 10 µM IAA at 4°C for 1 h. The incubation buffer used is 50 mM Tris-HCl (pH 7.5), 100 mM

NaCl, 10% glycerol, 10 μM MG132 and complete mini-protease inhibitors cocktail (Roche). Then 40 μL of Glutathione agarose (Thermo Scientific, 16102) was equilibrated, added into the reaction, and incubated for another 1 h at 4°C. Glutathione beads were recovered by a brief centrifugation and washed three times with 1 mL of washing buffer (50 mM Tris-HCl (pH 7.5), 100 mM NaCl, 10% glycerol, 0.1% Tween 20) containing the same amount of IAA as the incubation buffer. Western blot was performed as described above using Anti-HA-Peroxidase (Sigma, 12013819001) and anti-GST-tag, HRP-conjugated monoclonal antibody (Agrisera, AS18 4188).

Molecular docking

To carry out the molecular docking of ATP on TIR1, the published crystal structure available under PDB code 2P1Q was used[8]. Then crystallographic waters as well as the co-crystallized ASK1 adaptor protein were removed, and by using AutoDockTools[39] polar hydrogens were added to the structure and the file was converted to pdbqt format. Avogadro2[40] and OpenBabel[41] were used to draw the molecule of ATP, perform an initial geometry optimization, and protonate it for a pH of 7.4. Subsequently, a pdbqt file was created for ATP using AutoDockTools. Docking was performed using AutoDock Vina[42], which allows one to obtain results with high accuracy whilst retaining substantial speed. Because of the many degrees of freedom of the ATP molecule, a very high search exhaustiveness was used, to ensure that the whole conformational space was adequately sampled. Visualizations were created using UCSF Chimera[43]. Molecular surfaces were generated via MSMS[44], and the rendering was performed with PoV-Ray.

Microfluidic vRootchip and live imaging

The microfluidic vRootchip coupled to an in-house-established vertical Zeiss LSM 800 confocal microscope was used to analyze the rapid root growth inhibition, and monitor cytosolic Ca^{2+} level and apoplastic pH in real time, according to the previously established procedures in the lab[12,13]. The reported calcium senor GCaMP3[33] was crossed with the different homozygous transgenic lines generated in this study, and the F1 seedlings were directly used for imaging analysis. GFP (excitation, 488 nm; emission, 514 nm) signal in the epidermal cells of root elongation zone was captured every 15 s with a Plan-Apochromat ×20/0.8 NA air objective, and was then quantified using Image J. To measure apoplastic pH lively, a ratiometric fluorescent pH dye HPTS was added into the vRootchip medium at a final concentration of 1 mM. Fluorescence signals for protonated HPTS (excitation, 405 nm; emission, 514 nm) and deprotonated HPTS (excitation, 488 nm; emission, 514 nm) were detected with the same ×20/0.8 NA air objective. Image analysis was performed using batch processing of a previously described ImageJ macro[45].

Quantitative real-time PCR (qRT-PCR)

Five-days-old seedlings were transferred to ½ MS liquid medium (Mock) or medium containing 200 nM cvxIAA. Each treatment has 3 or 4 biological replicates. Seedlings were harvested at 3 h after treatment for RNA extraction with RNeasy Plant Mini Kit (QIAGEN, 74904). 1 μg of total RNA was used for reverse transcription after removal of genomic DNA according to the instructions of RevertAid First Strand cDNA Synthesis Kit (Thermo, K1622). cDNA was diluted 20 fold before qRT-PCR. Samples were pipetted in 3 technical replicates using an Automated Workstation Biomek i5 (Beckman Coulter). qRT-PCR was performed with LightCycler 480 (Roche) using Luna Universal qPCR Master Mix (NEB, M3003S). Sequences of the gene-specific primers used are all listed in Extended Data Table 1, and most

of them are actually directly taken from the previous publication[26]. Relative gene expression level was calculated using ΔΔCT method with Protein Phosphatase 2A Subunit A3 (PP2AA3) as the internal control.

Software and statistical analysis

Multiple sequence alignment was performed using the software Jalview[46]. The TIR1 3D structure (2p1q) was visualized and labelled in PDBe (Protein Data Bank in Europe). All graphs were generated using GraphPad Prism 8. One-way ANOVA, two-way ANOVA and multiple comparisons were performed where necessary using GraphPad Prism 8.

Methods references

32 Dharmasiri, N. et al. Plant development is regulated by a family of auxin receptor F box proteins. *Dev. Cell* **9**, 109-119 (2005).

33 Toyota, M. et al. Glutamate triggers long-distance, calcium-based plant defense signaling. *Science* **361**, 1112-1115 (2018).

34 Longair, M. H., Baker, D. A. & Armstrong, J. D. Simple Neurite Tracer: open source software for reconstruction, visualization and analysis of neuronal processes. *Bioinformatics* **27**, 2453-2454 (2011).

35 Li, L., Krens, S. F. G., Fendrych, M. & Friml, J. Real-time analysis of auxin response, cell wall pH and elongation in *Arabidopsis thaliana* hypocotyls. *Bio. Protoc.* **8**, e2685 (2018).

36 Lee, S. et al. Defining binding efficiency and specificity of auxins for $SCF^{TIR1/AFB}$-Aux/IAA co-receptor complex formation. *ACS Chem. Biol.* **9**, 673-682 (2014).

37 Quareshy, M. et al. The tetrazole analogue of the auxin indole-3-acetic acid binds preferentially to TIR1 and not AFB5. *ACS Chem. Biol.* **13**, 2585-2594 (2018).

38 Van Damme, T. et al. Wounding stress causes rapid increase in concentration of the naturally occurring 2',3'-isomers of cyclic guanosine- and cyclic adenosine monophosphate (cGMP and cAMP) in plant tissues. *Phytochemistry* **103**, 59-66 (2014).

39 Morris, G. M. et al. AutoDock4 and AutoDockTools4: Automated docking with selective receptor flexibility. *J. Comput. Chem.* **30**, 2785-2791 (2009).

40 Hanwell, M. D. et al. Avogadro: an advanced semantic chemical editor, visualization, and analysis platform. *J. Cheminform.* **4**, 17 (2012).

41 O'Boyle, N. M. et al. Open Babel: An open chemical toolbox. *J. Cheminform.* **3**, 33 (2011).

42 Trott, O. & Olson, A. J. AutoDock Vina: improving the speed and accuracy of docking with a new scoring function, efficient optimization, and multithreading. *J. Comput. Chem.* **31**, 455-461 (2010).

43 Pettersen, E. F. et al. UCSF Chimera--a visualization system for exploratory research and analysis. *J. Comput. Chem.* **25**, 1605-1612 (2004).

44 Sanner, M. F., Olson, A. J. & Spehner, J. C. Reduced surface: an efficient way to compute molecular surfaces. *Biopolymers* **38**, 305-320 (1996).

45 Barbez, E., Dunser, K., Gaidora, A., Lendl, T. & Busch, W. Auxin steers root cell expansion via apoplastic pH regulation in *Arabidopsis thaliana*. PNAS 114, E4884-E4893 (2017).

46 Waterhouse, A. M., Procter, J. B., Martin, D. M., Clamp, M. & Barton, G. J. Jalview Version 2--a multiple sequence alignment editor and analysis workbench. *Bioinformatics* **25**, 1189-1191 (2009).

Acknowledgements

This research was supported by the Life Science Facility (LSF) and the Bioimaging Facility (BIF) of IST Austria. We are grateful for the suggestions and advice from Chris Gehring, and the seeds and plasmids shared from Keiko U. Torii and Gary Stacey. This project was funded by the European Research Council Advanced Grant (ETAP-742985). M.F.K. and R.N. acknowledge the support of EU MSCA-IF project CrysPINs (792329). M.K. was supported by the project POWR.03.05.00 - 00 - Z302/17 Universitas Copernicana Thoruniensis in Futuro - IDS "Academia Copernicana". CIDG acknowledges support from UKRI under Future Leaders Fellowship grant number MR/T020652/1.

Author contributions

L.Q. and J.F. conceived and designed the experiments. L.Q. carried out most of the experiments. M.K. and K.J. performed most of the protein purification, *in vitro* AC activity assay and LC-MS/MS analysis. H.C. performed the vRootchip experiments. L.H. assisted with the root growth tracking with vertical microscope. M.Z. did the root gravitropism assay. S.S. originally tested relationship between auxin and eATP signaling. M.F.K. and R.N. assisted with TIR1 expression in insect cells. C.I.D.G. performed the molecular docking. L.Q. and J.F. wrote the manuscript.

Competing interests

The authors declare there are no competing interests.

Additional information and correspondence

All the main data supporting the conclusion of this study are available in the paper and its Extended Information. Additional data are available from the corresponding author upon reasonable request. Correspondence and material request should be addressed to J.F.

Extended Data Figure/Table Legends

Extended Data Figure 1. Additional data to support the AC activity of TIR1/AFBs

a-b, *E. coli* complementation assay showing that AFB1 and AFB5 have AC activity. The AC deficient SP850 strain was complemented with the empty vector (*pGEX-4T-1*), the positive control (HpAC1), and TIR1/AFBs. Red colour of the MacConkey Agar indicates the presence of AC activity (a). Western blot result shows that only AFB1 and AFB5 can be visibly detected among the 6 members of TIR1/AFBs. Ponceau red staining of the membrane was used as the loading control.

c, Michaelis-Menten kinetics for the AC activity of GST-AFB1 purified from *E. coli*. cAMP level after reaction was quantified by LC-MS/MS. S, substrate; V, velocity. For each data point, means ± SD from 3 biological replicates are shown.

d, Representative LC-MS/MS spectrum showing the detection of cAMP after the *in vitro* AC activity assay for His-GFP-FLAG-TIR1 purified from *Sf9* insect cells.

Extended Data Figure 2. Gel images showing the purity of all the proteins used

a, GST-AFB5. **b**, GST-AFB1. **c**, His-GFP-FLAG-TIR1. **d**, GST-PpAFB1. **e**, GST-PpAFB2. **f**, GST-PpAFB3. **g**, GST-PpAFB4. **h**, GST-AFB5$^{ACm1/m2/m3}$. **i**, GST-TIR1$^{\Delta NT}$. **j**, GST-TIR1$^{\Delta NT\text{-}ACm1/m2/m3}$. **k**, AFB5 after cleavage of GST tag. **l**, IAA7 after cleavage of GST tag. **m**, IAA17 after cleavage of GST tag. His-GFP-FLAG-TIR1 was purified from *Sf9* insect cells. All the other proteins were purified from BL-21 *E. coli* cells. Proteins were separated on SDS-PAGE gels and the gels were stained with Coomassie Brilliant Blue.

Extended Data Figure 3. AC activity is conserved in TIR1/AFBs orthologues from *Physcomitrella*

a, Alignment of the C-terminal protein sequences of TIR1/AFBs together with their orthologues from *Physcomitrella*. Note the AC motif is highly conserved in all the sequences. Only the first amino acid is a bit more relaxed.

b, TIR1/AFBs orthologues from *Physcomitrella* have AC activity. GST-tagged PpAFBs were purified from *E. coli*. *in vitro* AC activity assay was performed with GST as the negative control. cAMP level after reaction was quantified using LC-MS/MS. The values shown are means ± SD from 3 biological replicates. One-way ANOVA. ** $p \leqslant 0.01$; **** $p \leqslant 0.0001$.

Extended Data Figure 4. Protein structure of TIR1-IAA-Aux/IAA complex and ribbon structure showing ATP docking

a, Protein structure of TIR1-IAA-Aux/IAA complex showing the spatial position of the C-terminal AC motif. Different parts were labelled as different colours. Dark green, ASK1; Red, TIR1; White, C-terminal AC motif; Blue, IAA7 peptide; Yellow, $InsP_6$ (inositol hexakisphosphate); Green, IAA.

b, Ribbon structure showing the interaction of ATP with the key amino acids of the AC motif. AC center was labelled in magenta. E554 is the residue identified for m1 in Fig. 1a, R566 for m2, and D568 for m3. Note that V84 from the Aux/IAA degron restricts the space available to ATP.

Extended Data Figure 5. Auxin perception enhances the AC activity of AFB5

in vitro AC activity assay for AFB5 in the presence of 10 μM IAA, IAA7, IAA17 and the indicated combinations, followed by cAMP quantification using LC-MS/MS. Tag-cleaved clean proteins were used for this experiment. One-way ANOVA. n = 3. ** $p \leqslant 0.01$; **** $p \leqslant 0.0001$.

Extended Data Figure 6. Delayed requirement of the AC activity in root growth regulation

a, Loss of AC activity does not affect cvxIAA/ccvTIR1-induced root growth inhibition within the first hour. A vRootchip experiment was performed with the transgenic lines indicated, and the images were captured with a time interval of 1 min. Mock medium was changed to medium containing 500 nM of cvxIAA at 40 min. Root growth rate was normalized to the starting point of the respective group. n = 4.

b, Resistance of ccvTIR1^{ACm1} to cvxIAA-triggered root growth inhibition occurs only after 1 h of treatment. Vertical scanner growth assay was performed to track the root growth dynamics. Five-days-old seedlings of the indicated genotypes were transferred to either Mock medium or medium containing 200 nM of cvxIAA. Images were taken every 30 min. Root growth rate was measured. n = 10.

Extended Data Figure 7. TIR1 AC activity is not crucial for rapid auxin responses

a, cvxIAA triggers similar Ca^{2+} spikes in the *ccvTIR1* and *ccvTIR1^{ACm1}* lines. The calcium sensor GCaMP3 was crossed to the indicated transgenic lines. Five-days-old F1 seedlings were used for vRootchip experiment, and the images were captured with a time interval of 15 s. Mock medium was changed to medium containing 500 nM of cvxIAA at 10 min. The

fluorescence signal in the epidermal cells of root elongation zone was quantified, and was normalized to the average value of time points before treatment. n = 4.

b, Auxin-induced apoplastic alkalinisation is not changed in the *TIR1*^{ACm1} line. Five-days-old seedlings of the indicated genotypes were used for vRootchip experiment. Mock medium was changed to medium containing 10 nM of IAA at 11 min. Ratiometric (488 nm/405nm) imaging of HPST staining was used to measure apoplastic pH in the epidermal cells of root elongation zone. The values shown were normalized to the average of those time points before treatment. n = 4.

Extended Data Table 1. All the primes used in this study

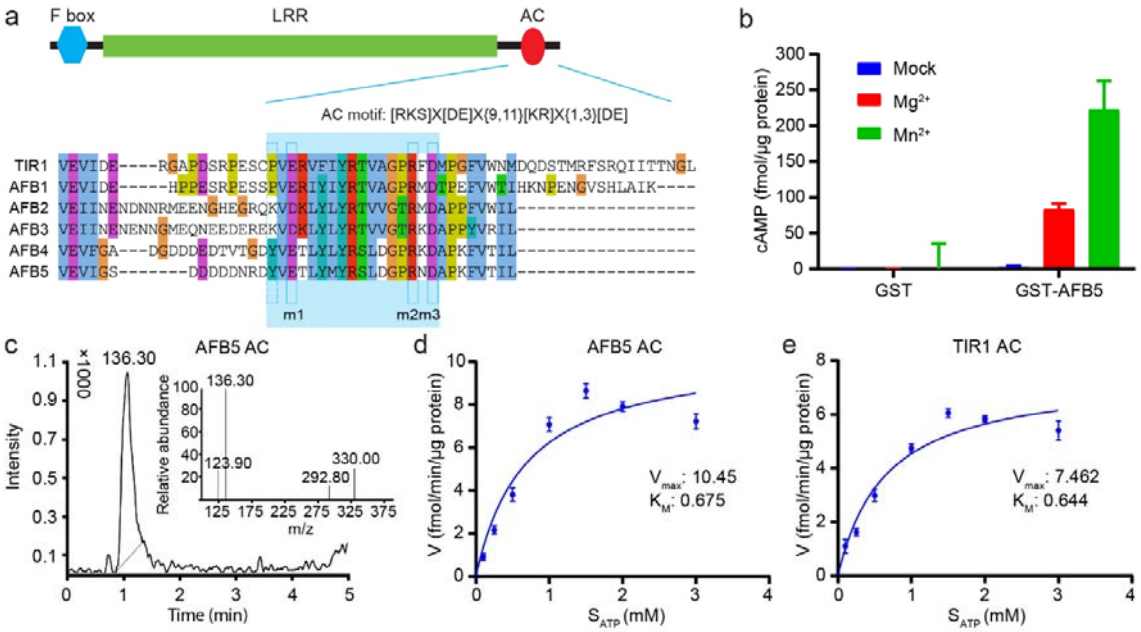

805

806 **Figure 1. TIR1/AFB auxin receptors have adenylate cyclase activity**

807 **a**, Alignment of the C-terminal protein sequences of TIR1/AFBs with the conserved AC motif.
808 LRR, leucine-rich repeat. The residues m1-m3 indicate the conserved key amino acids, which
809 were mutated to alanine to disrupt the AC activity (shown in Fig. 2).

810 **b-d**, *in vitro* AC activity of GST-AFB5 purified from *E.coli*. AC activity assay in the presence
811 of 2 different co-factors, followed by cAMP quantification by EIA (Enzyme ImmunoAssay)
812 kit. The values shown were blanked against the background signals from the corresponding
813 GST samples (**b**). Typical LC-MS/MS spectrum showing cAMP detection in the AC reaction
814 with the characteristic peak used for quantification (**c**). Michaelis-Menten kinetics for the AC
815 activity quantified by LC-MS/MS. S, substrate; V, velocity (**d**). For each data point, means ±
816 SD from 3 biological replicates are shown.

817 **e**, *in vitro* AC activity of His-GFP-FLAG-TIR1 purified from *Sf9* insect cells. Michaelis-
818 Menten kinetics giving results similar to GST-AFB5 (shown in d).

819

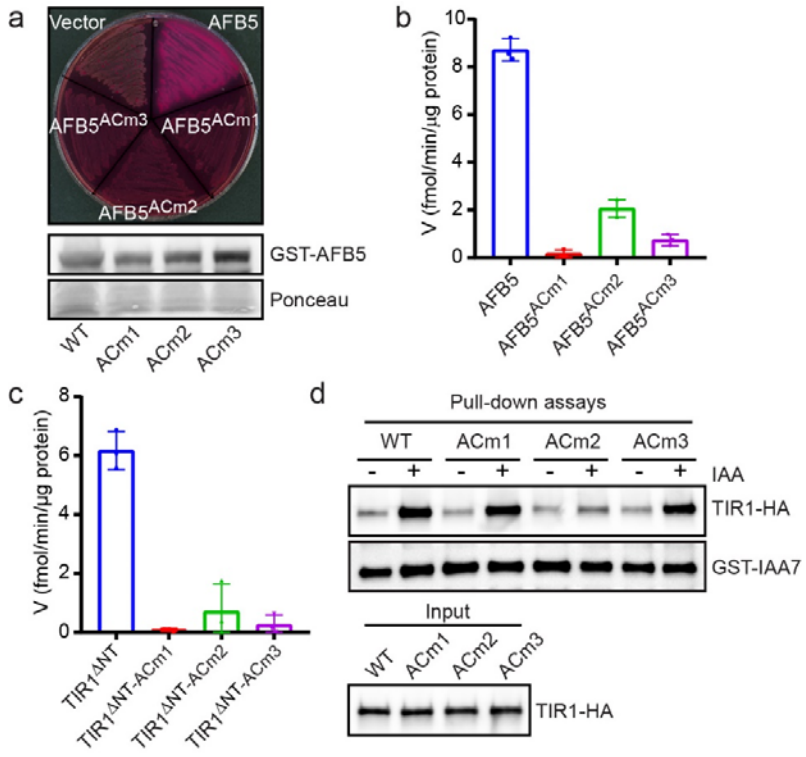

820

821 **Figure 2. C-terminal AC motif is responsible for the TIR1/AFB AC activity**

822 **a-b**, C-terminal AC motif is essential for the AFB5 AC activity. The AC deficient *E. coli* strain
823 SP850 was complemented by the indicated constructs. The red colour of the MacConkey agar
824 indicates the presence of AC activity. The empty vector *pGEX-4T-1* was used as negative
825 control. Western blot confirms similar expression levels of endogenous and mutated AFB5
826 proteins. Ponceau staining of the membrane was used as the loading control (**a**). *in vitro* AC
827 activity assay for the purified GST-AFB5 and 3 mutated variants, followed by the cAMP
828 quantification using LC-MS/MS. V, velocity. The values shown are means ± SD from 3
829 biological replicates (**b**).

830 **c**, C-terminal AC motif is essential for the AC activity of TIR1$^{\Delta NT}$. GST-TIR1$^{\Delta NT}$ and 3
831 mutated variants were purified from *E. coli*. An *in vitro* AC activity assay was performed
832 followed by cAMP quantification using LC-MS/MS. V, velocity. The values shown are means
833 ± SD from 3 biological replicates.

d, Pull-down results showing differential effects of TIR1^{ACm} mutations on the IAA-induced TIR1-Aux/IAA interaction. Wild-type and the 3 mutated TIR1 variants were translated *in vitro* using wheat germ extracts, and were then used for pull-down assays with purified GST-IAA7, in the presence or absence of 10 μM IAA as indicated.

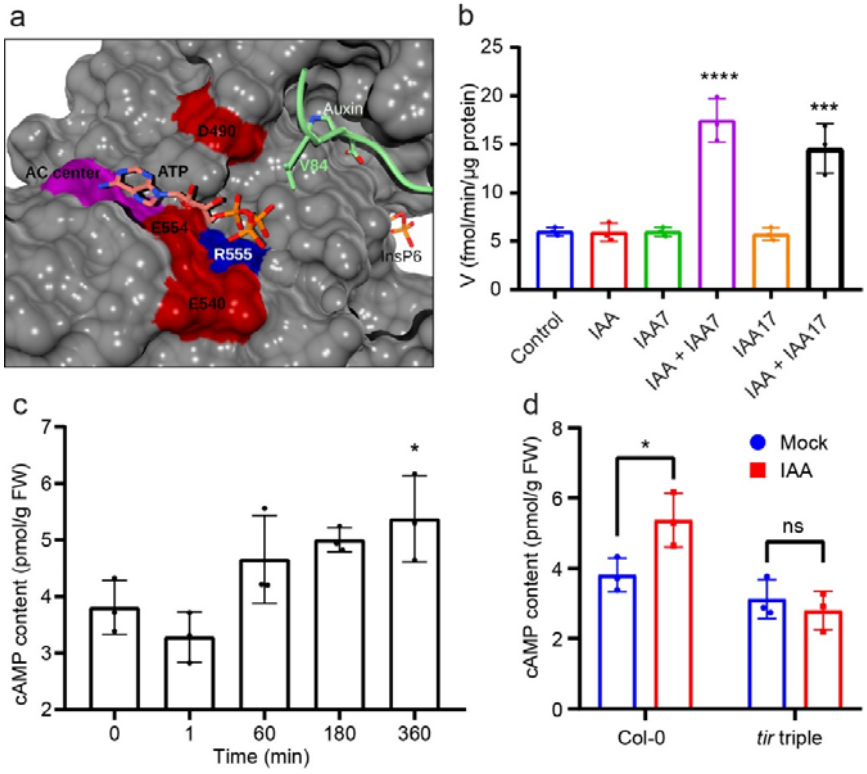

839

840 **Figure 3. Auxin perception enhances the TIR1/AFBs AC activity**

841 **a**, Docking of ATP on the surface of TIR1-IAA-Aux/IAA complex. The beginning of the AC
842 center was labelled in magenta. Amino acids presumably important for the AC activity were
843 labelled either in red (acidic), or in blue (basic). E554 is the site for m1 (as in Fig. 1a). Note
844 that V84 from the Aux/IAA degron restricts the space available to ATP.

845 **b**, Auxin together with Aux/IAA stimulates the TIR1 AC activity. *in vitro* AC activity assay
846 with His-GFP-FLAG-TIR1 (5 μg) in the presence of 10 μM IAA, IAA7 (3 μg), IAA17 (3 μg)
847 and the indicated combinations, followed by cAMP quantification using LC-MS/MS. V,
848 velocity. One-way ANOVA. n = 3. *** $p \leqslant 0.001$; **** $p \leqslant 0.0001$.

849 **c**, Auxin treatment increases cAMP content in root tissues . Five-days-old Col-0 seedlings were
850 treated with 100 nM IAA. Root tissues were harvested for cAMP quantification by LC-MS/MS.
851 One-way ANOVA. n = 3. * $p \leqslant 0.05$.

852 **d**, Auxin-induced increase of cAMP levels in roots is dependent on TIR1/AFBs. Five-days-old
853 Col-0 or *tir* triple seedlings were treated with 100 nM IAA for 6 h. Root tissues were collected
854 for cAMP measurement by LC-MS/MS. One-way ANOVA. n = 3. * $p \leqslant 0.05$. ns, not
855 significant.

856

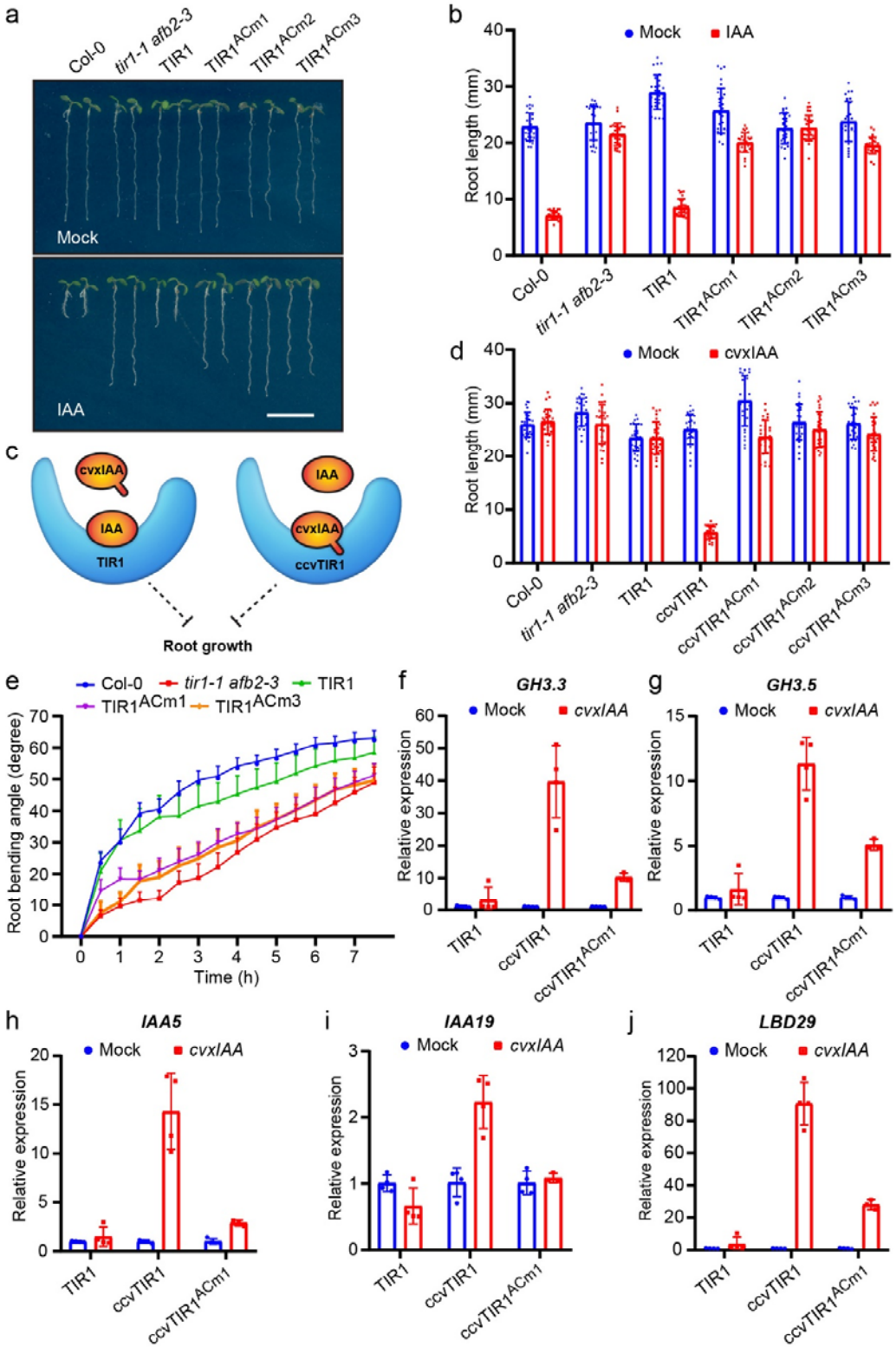

857

858 **Figure 4. TIR1 AC activity contributes to auxin-induced root growth inhibition and**

859 **transcriptional responses**

a-b, AC motif mutations compromise TIR1 function in mediating IAA-induced root growth inhibition. *pTIR1::TIR1* and the similar constructs containing the 3 AC motif mutations were transformed into *tir1-1 afb2-3*. Representative examples of 6-days-old seedlings of different genotypes grown on Mock or 100 nM IAA containing medium. Bar = 10 mm (**a**). Quantification of the root length in (a). n = 30 (**b**).

c, Simplified scheme showing the principles of the engineered cvxIAA/ccvTIR1 system.

d, C-terminal AC motif is crucial for cvxIAA-triggered root growth inhibition in *ccvTIR1* line. *pTIR1::TIR1*, *pTIR1::ccvTIR1*, and the 3 similar constructs containing the AC motif mutations (see Fig. 1a) were transformed into *tir1-1 afb2-3*. Root length of the 6-days-old seedlings with different genotypes grown on Mock or 500 nM cvxIAA containing medium were measured. n = 30.

e, AC activity is required for TIR1 function in root gravitropism. Five-days-old seedlings of the indicated genotypes were transferred to new plates. The plates were rotated 90 degree before images were captured every 30 min. Root bending angle was measured to monitor the gravitropic response. n = 10.

f-j, AC activity contributes to auxin-induced genes expression. Five-days-old seedlings were either Mock-treated or treated with liquid medium containing 200 nM cvxIAA for 3 h. Seedlings were harvested for RNA extraction and qRT-PCR. Shown are the relative expression values normalized to the internal control *PP2AA3*, from 3 or 4 biological replicates.

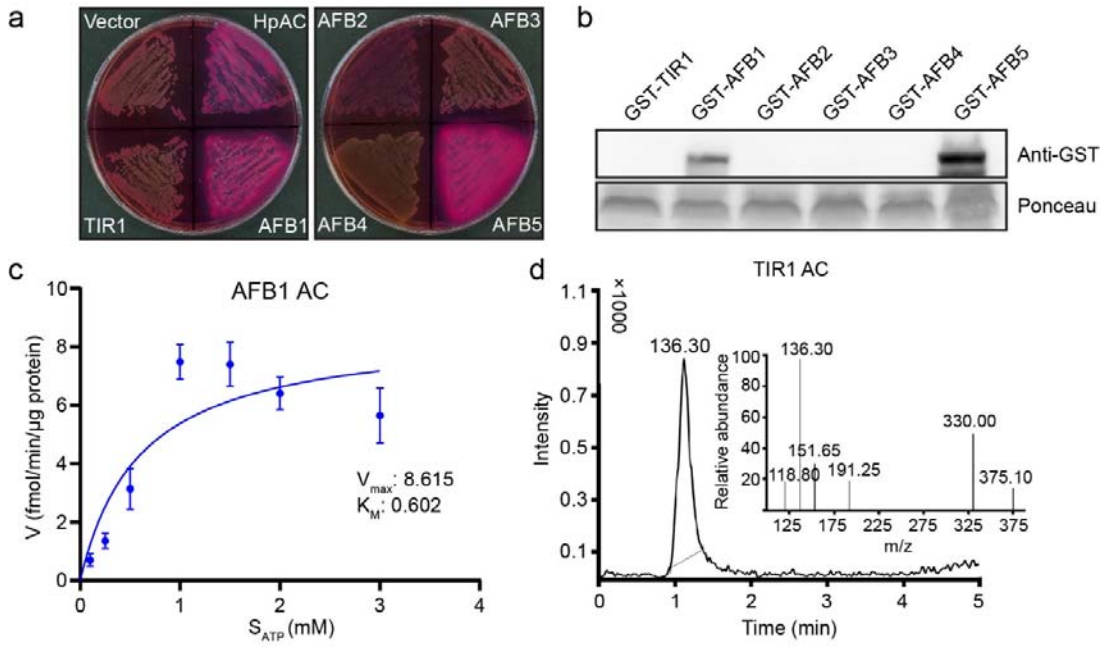

880

881 **Extended Data Figure 1. Additional data to support the AC activity of TIR1/AFBs**

882 **a-b**, *E. coli* complementation assay showing that AFB1 and AFB5 have AC activity. The AC
883 deficient SP850 strain was complemented with the empty vector (*pGEX-4T-1*), the positive
884 control (HpAC1), and TIR1/AFBs. Red colour of the MacConkey Agar indicates the presence
885 of AC activity (a). Western blot result shows that only AFB1 and AFB5 can be visibly detected
886 among the 6 members of TIR1/AFBs. Ponceau red staining of the membrane was used as the
887 loading control.

888 **c**, Michaelis-Menten kinetics for the AC activity of GST-AFB1 purified from *E. coli*. cAMP
889 level after reaction was quantified by LC-MS/MS. S, substrate; V, velocity. For each data point,
890 means ± SD from 3 biological replicates are shown.

891 **d**, Representative LC-MS/MS spectrum showing the detection of cAMP after the *in vitro* AC
892 activity assay for His-GFP-FLAG-TIR1 purified from *Sf9* insect cells.

893

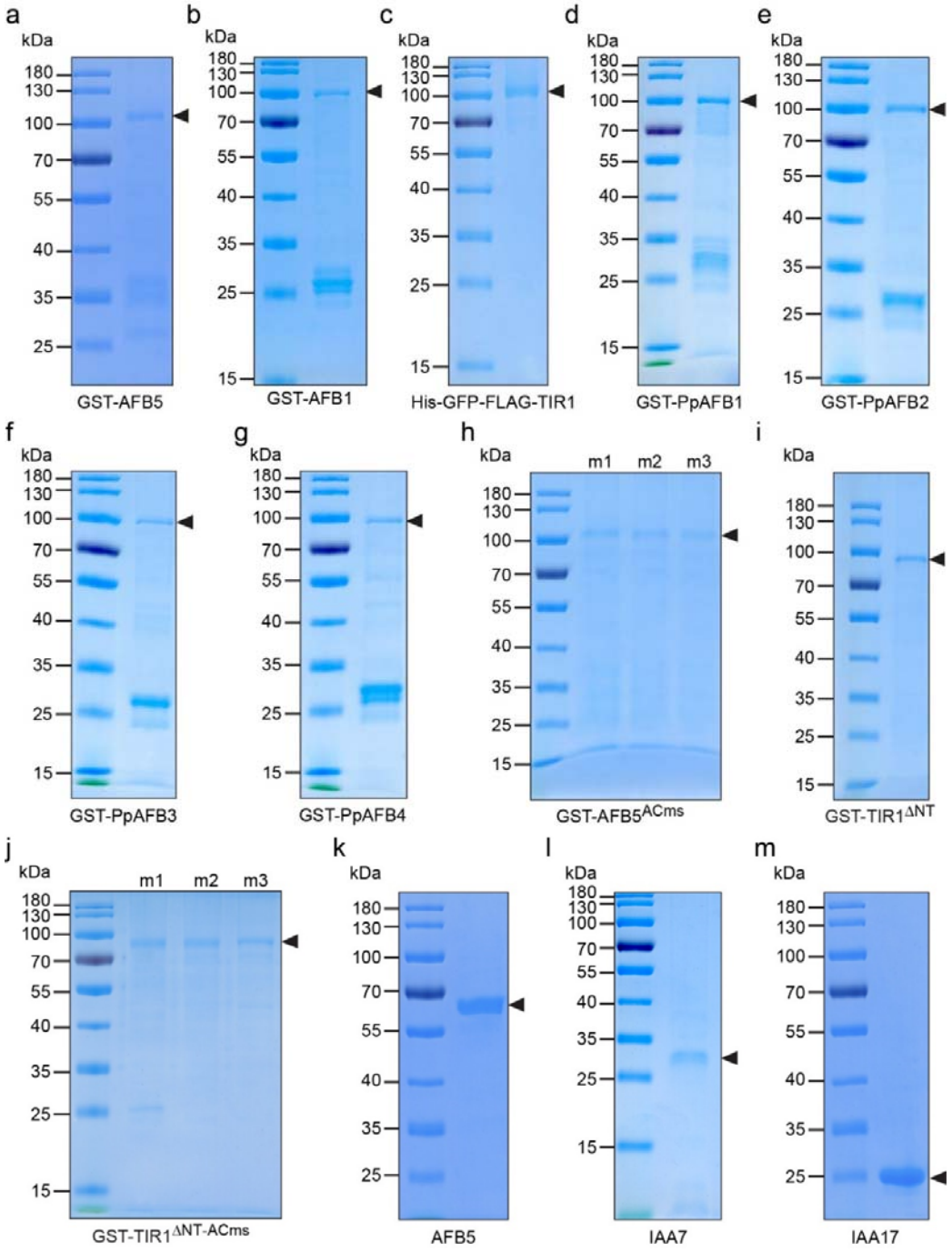

894

895 **Extended Data Figure 2. Gel images showing the purity of all the proteins used**

896 **a**, GST-AFB5. **b**, GST-AFB1. **c**, His-GFP-FLAG-TIR1. **d**, GST-PpAFB1. **e**, GST-PpAFB2. **f**,

897 GST-PpAFB3. **g**, GST-PpAFB4. **h**, GST-AFB5$^{ACm1/m2/m3}$. **i**, GST-TIR1$^{\Delta NT}$. **j**, GST-TIR1$^{\Delta NT-}$

898 $^{ACm1/m2/m3}$. **k**, AFB5 after cleavage of GST tag. **l**, IAA7 after cleavage of GST tag. **m**, IAA17

after cleavage of GST tag. His-GFP-FLAG-TIR1 was purified from *Sf9* insect cells. All the other proteins were purified from BL-21 *E. coli* cells. Proteins were separated on SDS-PAGE gels and the gels were stained with Coomassie Brilliant Blue.

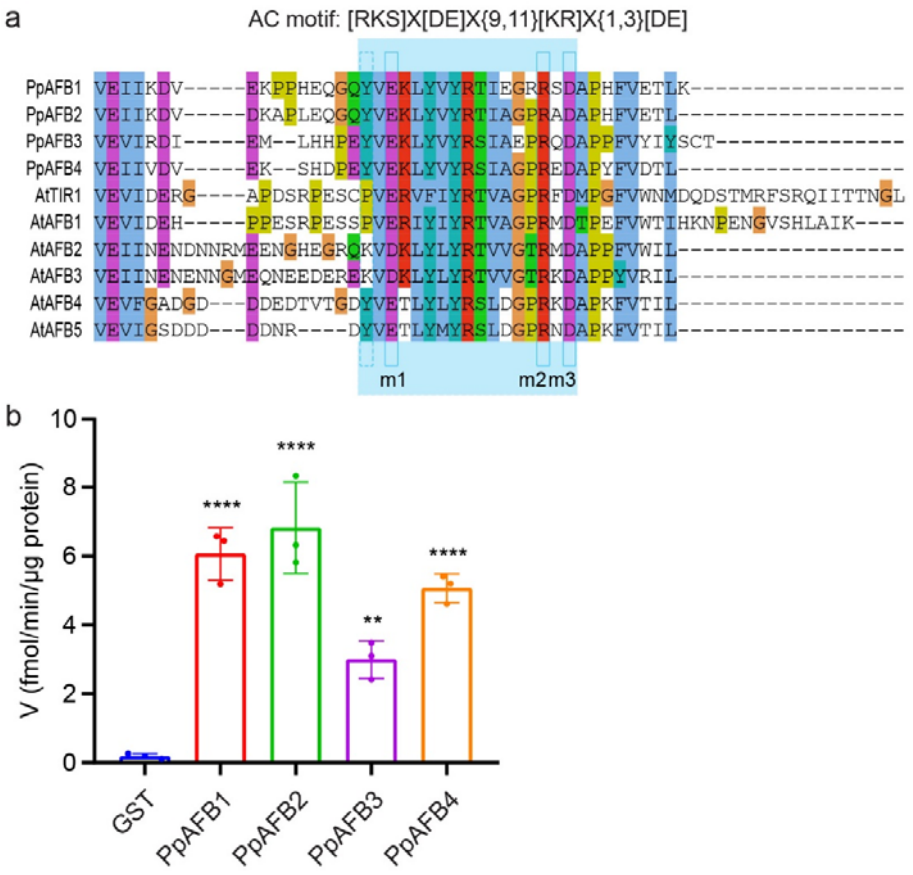

903

904 **Extended Data Figure 3. AC activity is conserved in TIR1/AFBs orthologues from**

905 ***Physcomitrella***

906 **a**, Alignment of the C-terminal protein sequences of TIR1/AFBs together with their

907 orthologues from *Physcomitrella*. Note the AC motif is highly conserved in all the sequences.

908 Only the first amino acid is a bit more relaxed.

909 **b**, TIR1/AFBs orthologues from *Physcomitrella* have AC activity. GST-tagged PpAFBs were

910 purified from *E. coli*. *in vitro* AC activity assay was performed with GST as the negative

911 control. cAMP level after reaction was quantified using LC-MS/MS. The values shown are

912 means ± SD from 3 biological replicates. One-way ANOVA. ** $p \leqslant 0.01$; **** $p \leqslant 0.0001$.

913

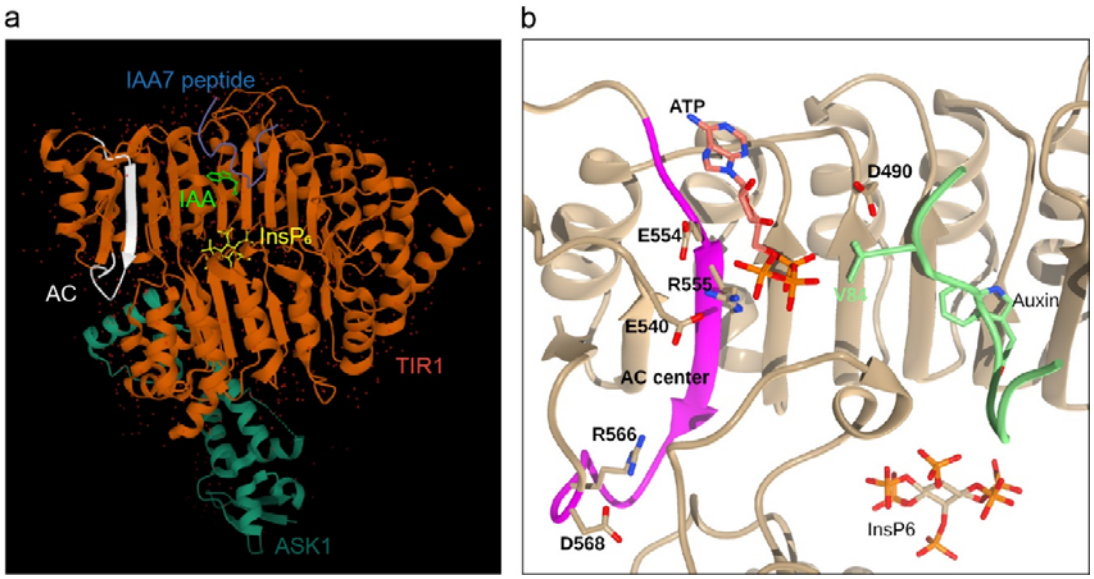

914

915 **Extended Data Figure 4. Protein structure of TIR1-IAA-Aux/IAA complex and ribbon**

916 **structure showing ATP docking**

917 **a**, Protein structure of TIR1-IAA-Aux/IAA complex showing the spatial position of the C-

918 terminal AC motif. Different parts were labelled as different colours. Dark green, ASK1; Red,

919 TIR1; White, C-terminal AC motif; Blue, IAA7 peptide; Yellow, $InsP_6$ (inositol

920 hexakisphosphate); Green, IAA.

921 **b**, Ribbon structure showing the interaction of ATP with the key amino acids of the AC motif.

922 AC center was labelled in magenta. E554 is the residue identified for m1 in Fig. 1a, R566 for

923 m2, and D568 for m3. Note that V84 from the Aux/IAA degron restricts the space available to

924 ATP.

925

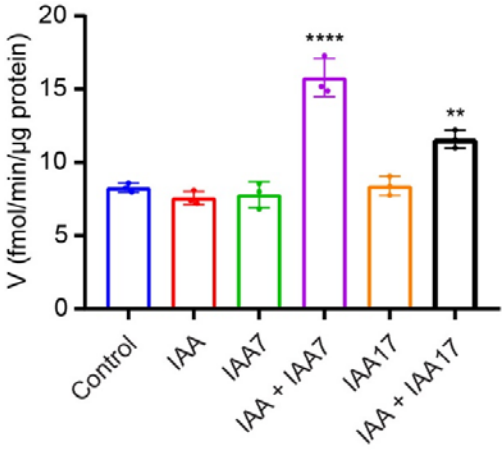

926

927 **Extended Data Figure 5. Auxin perception enhances the AC activity of AFB5**

928 *in vitro* AC activity assay for AFB5 in the presence of 10 µM IAA, IAA7, IAA17 and the
929 indicated combinations, followed by cAMP quantification using LC-MS/MS. Tag-cleaved
930 clean proteins were used for this experiment. One-way ANOVA. n = 3. ** $p \leqslant 0.01$; **** $p \leqslant$
931 0.0001.

932

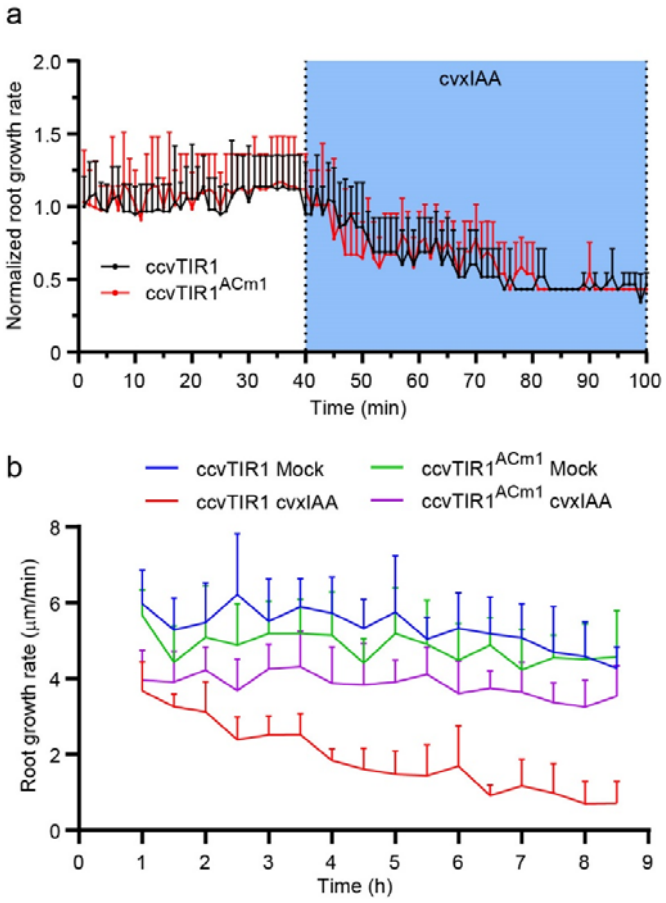

933

934 **Extended Data Figure 6. Delayed requirement of the AC activity in root growth**

935 **regulation**

936 **a**, Loss of AC activity does not affect cvxIAA/ccvTIR1-induced root growth inhibition within

937 the first hour. A vRootchip experiment was performed with the transgenic lines indicated, and

938 the images were captured with a time interval of 1 min. Mock medium was changed to medium

939 containing 500 nM of cvxIAA at 40 min. Root growth rate was normalized to the starting point

940 of the respective group. n = 4.

941 **b**, Resistance of ccvTIR1^{ACm1} to cvxIAA-triggered root growth inhibition occurs only after 1

942 h of treatment. Vertical scanner growth assay was performed to track the root growth dynamics.

943 Five-days-old seedlings of the indicated genotypes were transferred to either Mock medium or

944 medium containing 200 nM of cvxIAA. Images were taken every 30 min. Root growth rate
945 was measured. n = 10.
946

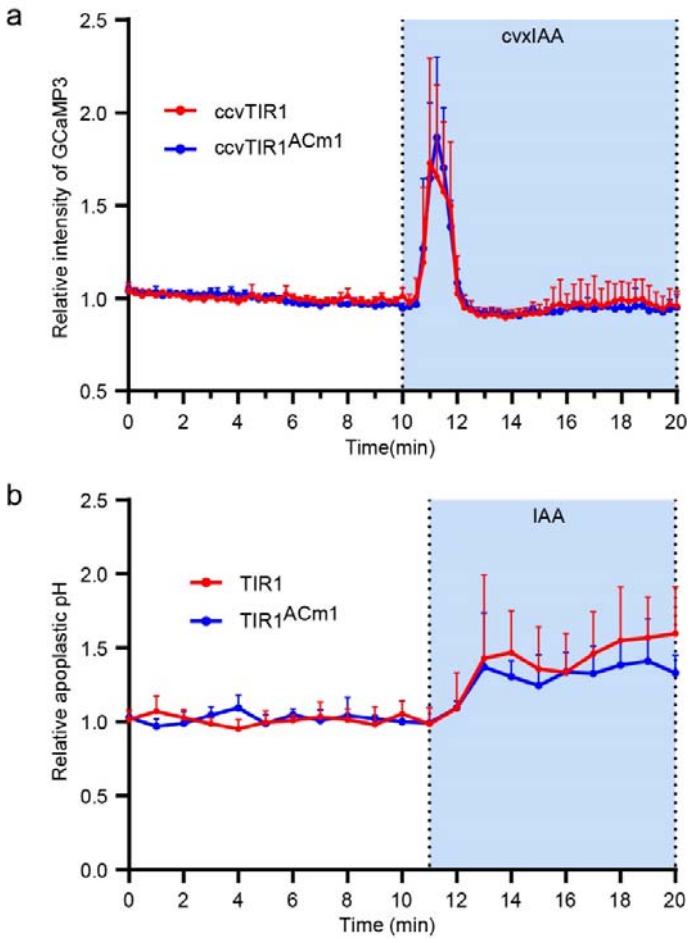

947

948 **Extended Data Figure 7. TIR1 AC activity is not crucial for rapid auxin responses**

949 **a**, cvxIAA triggers similar Ca^{2+} spikes in the *ccvTIR1* and *ccvTIR1*^{ACm1} lines. The calcium
950 sensor GCaMP3 was crossed to the indicated transgenic lines. Five-days-old F1 seedlings were
951 used for vRootchip experiment, and the images were captured with a time interval of 15 s.
952 Mock medium was changed to medium containing 500 nM of cvxIAA at 10 min. The
953 fluorescence signal in the epidermal cells of root elongation zone was quantified, and was
954 normalized to the average value of time points before treatment. n = 4.

955 **b**, Auxin-induced apoplastic alkalinisation is not changed in the *TIR1*^{ACm1} line. Five-days-old
956 seedlings of the indicated genotypes were used for vRootchip experiment. Mock medium was
957 changed to medium containing 10 nM of IAA at 11 min. Ratiometric (488 nm/405nm) imaging

958 of HPST staining was used to measure apoplastic pH in the epidermal cells of root elongation
959 zone. The values shown were normalized to the average of those time points before treatment.
960 n = 4.

961

962 **Extended Data Table 1. All the primes used in this study**

Primers	Sequences	Usage
tir1-1-GT-FP	AGCGACGGTGATTAGGAGGT (CAPS, digestion with Bsa Ⅰ)	Genotyping
tir1-1-GT-RP	CAGGAACAACGCAGCAAAA	
afb2-3-GT-FP	TTCTCCTTCGATCATTGTCAAC	
afb2-3-GT-RP	TAGCGGCAATAGAGGCAAGA	
LBb1.3	ATTTTGCCGATTTCGGAAC (for SALK lines)	
TIR1-pGEX-FP	CGCGGATCCATGCAGAAGCGAATAGCCTTG (BamHI)	Protein expression in *E. coli*
TIR1-pGEX-RP	ACGCGTCGACTTATAATCCGTTAGTAGTAATGATTTGCC (SalI)	
AFB1-pGEX-FP	CGCGGATCCATGGGTCTCCGATTCCCACCT (BamHI)	
AFB1-pGEX-RP	ACGCGTCGACTTACTTTATGGCTAGATGTGAAACTCCATTC (SalI)	
AFB2-pGEX-FP	CGCGGATCCATGAATTATTTCCCAGATGAAGTAATAGAG (BamHI)	
AFB2-pGEX-RP	ACGCGTCGACTTAGAGAATCCACACAAATGGCG (SalI)	
AFB3-pGEX-FP	CGCGGATCCATGAATTATTTCCCAGACGAGGTT (BamHI)	
AFB3-pGEX-RP	ACGCGTCGACCTAAAGAATCCTAACATATGGTGGTG (SalI)	
AFB4-pGEX-FP	CGCGGATCCATGACAGAAGAAGATAGCTCAGC (BamHI)	
AFB4-pGEX-RP	ACGCGTCGACTCATAAAATTGTTACAAACTTTGGAGC (SalI)	
AFB5-pGEX-FP	CGCGGATCCATGACACAAGATCGCTCAGAAATG (BamHI)	
AFB5-pGEX-RP	CCGCTCGAGCTATAAAATCGTGACGAACTTTGGT (XhoI)	
TIR1 ΔNT -pGEX-FP	CGCGGATCCCTTGAAGAGATAAGGCTGAAGAGGA (BamHI)	
IAA7-pGEX-FP	CGCGGATCCATGATCGGCCAACTTATGAACC (BamHI)	

IAA7-pGEX-RP	ACGCGTCGACTCAAGATCTGTTCTTGCAGTACT TCTC (SalI)	
IAA17-pGEX-FP	CGCGGATCCATGATGGGCAGTGTCGAGCTG (BamHI)	
IAA17-pGEX-RP	CCGCTCGAGTCAAGCTCTGCTCTTGCACTTCTC (XhoI)	
TIR1p-B4-FP	GGGGACAACTTTGTATAGAAAAGTTGGAGGCT AAAAATAAATGCGGAAAAAAG (AttB4)	Transgenic plants
TIR1p-B1r-RP	GGGGACTGCTTTTTTGTACAAACTTGTTGCGGC CAAATAACCTCGAG (AttB1r)	
TIR1-B1-FP	GGGGACAAGTTTGTACAAAAAAGCAGGCTTCA TGCAGAAGCGAATAGCCTTG (AttB1)	
TIR1-B2-RP	GGGGACCACTTTGTACAAGAAAGCTGGGTTTTA TAATCCGTTAGTAGTAATGATTTGCC (AttB2)	
TIR1-ccv-FP	GAAAACCTCACGGTGCTGACTTTAATTTG	ccvTIR1 mutation
TIR1-ccv-RP	CTTTAAGCTCCACGGATCTCACTTTC	
TIR1-ACm1-FP	CTGCCCTGTTGCGAGAGTCTTCATATAC	TIR1 AC motif mutations
TIR1-ACm1-RP	CTCTCTGGTCTCGAGTCCGGTG	
TIR1-ACm2-FP	TGGCTGGTCCTGCATTTGACATGC	
TIR1-ACm2-RP	CTGTTCGGTATATGAAGACTCTCTCAACAG	
TIR1-ACm3-FP	TCCTCGATTTGCCATGCCTGGCT	
TIR1-ACm3-RP	CCAGCCACTGTTCGGTATATGAAGAC	
AFB5-ACm1-FP	AGGGATTATGTCGCTACTTTATACATGTATC	AFB5 AC motif mutations
AFB5-ACm1-RP	ATTGTCATCATCATCATCCGATCC	
AFB5-ACm2-FP	CTTGATGGTCCAGCTAATGATGCACC	
AFB5-ACm2-RP	AGACCGATACATGTATAAAGTCTCGAC	
AFB5-ACm3-FP	GTCCAAGGAATGCTGCACCAAAGTTC	
AFB5-ACm3-RP	CATCAAGAGACCGATACATGTATAAAGTC	
pGEX-S-F	GGGCTGGCAAGCCACGTTTGGTG	Sequencing
pGEX-S-R	CCGGGAGCTGCATGTGTCAGAGG	
TIR1p-S-F1	CCACACTTCTCCCATCTGACTAT	
M13-21F	TGTAAAACGACGGCCAGT	
M13-29R	CAGGAAACAGCTATGACC	
PP2AA3-q-FP	TAACGTGGCCAAAATGATGC	qRT-PCR
PP2AA3-q-RP	GTTCTCCACAACCGCTTGGT	
GH3.3-q-FP	CATCACAGAGTTCCTCACAAGC	
GH3.3-q-RP	GTCGGTCCATGTCTTCATCA	

GH3.5-q-FP	CATCTCTGAGTTCCTCACAAGC	
GH3.5-q-RP	CCTCTTCGATTGTTGGCATT	
IAA5-q-FP	TGAAGGAAAGTGAATGTGTACCAA	
IAA5-q-RP	GCACGATCCAAGGAACATTT	
IAA19-q-FP	TGGTGACAACTGCGAATACGTTAC	
IAA19-q-RP	CGTCTACTCCTCTAGGCTGCAG	
LBD29-q-FP	GCTAGGCTTCAAGATCCCATC	
LBD29-q-RP	TGTGCTGCTTGTTGCTTTAGA	

963
964

965